AGU PUBLICATIONS

JGR

Journal of Geophysical Research: Earth Surface

RESEARCH ARTICLE
10.1002/2015JF003699

Key Points:
- Presents energetics-based formulation for the evolution of sandy wave-dominated profiles
- Derives estimation of a temporally defined morphodynamic depth of closure
- Important to use linear Airy wave theory versus shallow water wave assumptions

Supporting Information:
- Text S1 and Figures S1–S4
- Figure S1
- Figure S2
- Figure S3
- Figure S4

Correspondence to:
A. C. Ortiz,
aortiz@whoi.edu

Citation:
Ortiz, A. C., and A. D. Ashton (2016), Exploring shoreface dynamics and a mechanistic explanation for a morphodynamic depth of closure, *J. Geophys. Res. Earth Surf.*, *121*, 442–464, doi:10.1002/2015JF003699.

Received 18 AUG 2015
Accepted 9 JAN 2016
Accepted article online 13 JAN 2016
Published online 27 FEB 2016

Exploring shoreface dynamics and a mechanistic explanation for a morphodynamic depth of closure

Alejandra C. Ortiz[1,2] and Andrew D. Ashton[1]

[1]Department of Geology and Geophysics, Woods Hole Oceanographic Institution, Woods Hole, Massachusetts, USA, [2]Department of Earth, Atmospheric, and Planetary Science, Massachusetts Institute of Technology, Cambridge, Massachusetts, USA

Abstract Using energetics-based formulations for wave-driven sediment transport, we develop a robust methodology for estimating the morphodynamic evolution of a cross-shore sandy coastal profile. In our approach, wave-driven cross-shore sediment flux depends on three components: two onshore-directed terms (wave asymmetry and wave streaming) and an offshore-directed slope term. In contrast with previous work, which applies shallow water wave assumptions across the transitional zone of the lower shoreface, we use linear Airy wave theory. The cross-shore sediment transport formulation defines a dynamic equilibrium profile and, by perturbing about this steady state profile, we present an advection-diffusion formula for profile evolution. Morphodynamic Péclet analysis suggests that the shoreface is diffusionally dominated. Using this depth-dependent characteristic diffusivity timescale, we distinguish a morphodynamic depth of closure for a given time envelope. Even though wave-driven sediment transport can (and will) occur at depths deeper than this morphodynamic closure depth, the rate of morphologic bed changes in response to shoreline change becomes asymptotically slow. Linear wave theory suggests a shallower shoreface depth of closure and much sharper break in processes than shallow water wave assumptions. Analyzing hindcasted wave data using a weighted frequency-magnitude approach, we determine representative wave conditions for selected sites along the U.S. coastline. Computed equilibrium profiles and depths of closure demonstrate reasonable similarities, except where inheritance is strong. The methodology espoused in this paper can be used to better understand the morphodynamics at the lower shoreface transition with relative ease across a variety of sites and with varied sediment transport equations.

1. Introduction

The wave-affected shoreface represents a transitional zone between the shoreline and the continental shelf. The dynamics of the shoreface and the definition of the lower "shoreface toe" or "wave base" are relevant across a wide range of coastal sciences, spanning sedimentology, coastal geology, and coastal engineering. Delineation and estimation of the lower shoreface transition are typically explicit in many models of coastal evolution, from the simple Bruun rule [*Bruun*, 1962] to barrier island translation models [*Cowell et al.,* 1995; *Stolper et al.,* 2005; *Moore et al.,* 2010; *Lorenzo-Trueba and Ashton*, 2014] and even in engineering estimations of beach nourishment design volumes [*Dean*, 2002]. The mechanisms, rates, and depths of wave-driven sediment exchange are important across many coastal settings, including sandy coasts [*Bruun*, 1988; *Ranasinghe et al.,* 2012], barrier islands [*Moore et al.,* 2010; *Lorenzo-Trueba and Ashton*, 2014], wave-influenced deltas [*Swenson et al.,* 2005; *Ashton and Giosan*, 2011], and even cliffed coasts fronted by sandy beaches [*Bray and Hooke*, 1997; *Dickson et al.,* 2009; *Ashton et al.,* 2011; *Limber et al.,* 2014].

With sea level rise rates becoming faster than they have been over the past several millennia [*Vermeer and Rahmstorf*, 2009], the shoreface dynamics of wave-dominated coasts needs to be better understood to enable predictions of future coastal evolution. Just as important as understanding the potential for onshore or offshore sediment transport between the upper and lower shoreface [*Aagaard*, 2014] is an understanding of how changes in the upper shoreface are morphologically communicated offshore. The myriad processes that can change coastlines, from overwash [*Donnelly et al.,* 2006; *Sherwood et al.,* 2014] to alongshore sediment transport gradients [*Ashton and Murray*, 2006] or even human activities such as beach nourishment [*Jin et al.,* 2013], motivate a better understanding of how the shoreface behaves as a morphologic unit. The focus of this study is the development of a formulation for the long-term morphodynamic evolution

of a sandy wave-dominated shoreface. Our goal is to present methodologies that can better explain and quantify long-term shoreface evolution, emphasizing the dynamics of the lower shoreface rather than the surf zone and upper shoreface, which have characteristic response times much more rapid than sea level rise rates.

2. Background

2.1. Depth of Closure, Wave Base, and the Shoreface Toe

The wave-dominated inner shelf has long been the subject of scientific investigation [*Komar*, 1991; *Wright et al.,* 1991], and it has long been understood that shoreface slopes develop as a balance between onshore and offshore sediment transport processes [*Fenneman*, 1902]. In this paper, we use the term shoreface to describe several subdivisions of the shoreface including the surf zone, upper shoreface, lower shoreface, inner shelf, and midshelf. The upper shoreface includes the region where the effects of wave energy dissipation dominate, while the lower shoreface is dominated by bed interactions from shoaling waves [*Stive and de Vriend*, 1995]. Perhaps one of the most debated subjects in coastal science is the concept of the depth of shoreface closure. Regardless of the specific definition, there is a general agreement that there exists an offshore transition whereby wave influence on bed stresses, and therefore sediment transport, becomes significantly smaller than within the surf zone or upper shoreface.

Sedimentologists and stratigraphers define the wave base as the depth to which waves interact with the bed [*Nichols*, 1999]. This transition can be seen in sedimentary sequences, often accompanied by changes in sediment characteristics and preserved bedforms—the location of this transition may be called the shoreface toe [*Dean and Maurmeyer*, 1983]. *Swift et al.* [1985] defined the shoreface toe as a geometric slope break, reflecting an implied change in geologic processes. Observations of sediment texture along nourished beaches suggest an offshore limit to vigorous onshore and offshore sediment exchange but one that is deeper than typically predicted by depth of closure arguments [*Thieler et al.,* 1995]. Sedimentological approaches also often distinguish the fair-weather wave base as the depth at which the background wave climate interacts with the bed. This transition is associated with a change in sedimentary structures and bedforms from wave ripples and dunes to hummocky cross stratification [*Dott and Bourgeois*, 1982; *Duke*, 1985; *McCave*, 1985]. Likewise, the depth at which mean storm waves interact with the bed defines the storm wave base and is also associated with a change in bed sedimentology and bedforms from hummocky cross stratification to mostly muddy or silty sediments [*Sageman*, 1996]. Often, the end of upper shoreface and transition to the lower shoreface is defined as the depth of the fair-weather wave base, while the transition between the lower shoreface and offshore is defined as the storm wave base [*Dean and Dalrymple*, 1991; *Nichols*, 1999]. However, recently, *Peters and Loss* [2012] suggested that based upon wave height distributions, modern open ocean wave climates may not clearly distinguish between fair-weather and storm conditions, questioning the fair versus storm wave distinction often applied to sedimentary records.

In engineering practice, the "depth of closure" or "closeout depth" [*Birkemeier*, 1985] is often used to define a short-term (1–10 years) limit of annual/interseasonal bed change. *Hallermeier* [1978] computed the depth of closure as the "maximum water depth for intense bed agitation," which he defines as the wave conditions that are exceeded 12 h each year. Often, closure depth is also inferred as the seaward limit of measurable shoreface depth change [*Hallermeier*, 1978; *Birkemeier*, 1985; *Nicholls et al.,* 1996]. *Wright et al.* [1991], however, argued that bed changes (or the lack thereof) at the depth of closure must be measurable at the rate of bed accumulation equal to local relative sea level rise rates—for most coasts this would require measurements with subcentimeter accuracy to capture rates of a few mm/yr [*Kemp et al.,* 2011].

Closure depths computed following the approaches of *Hallermeier* [1978] and *Birkemeier* [1985] typically range from 5 to 10 m. These computed depths of closure are shallower than those inferred from geological evidence of the shoreface transition and active wave reworking and may only apply for annual to decadal scales [*Thieler et al.,* 1995; *Wallace et al.,* 2010]. As discussed by *Stive et al.* [1991], the relevant depth of closure should increase with an increase in timescale considered. Additionally, the shoreface toe may not represent a true "sediment fence," as some studies suggest long-term onshore transport across the shoreface toe [*Stive and de Vriend*, 1995; *Aagaard*, 2014].

2.2. Shoreface Response to Sea Level Rise

The Bruun Rule [*Bruun*, 1962], which quantifies and visualizes shoreline translation assuming geometric rules, offers perhaps the most straightforward conceptualization of shoreface response to sea level rise. If a concave

offshore profile retains its shape and there is a shoreface toe, the entire shoreface profile is assumed to respond as sea level rises and, due to mass conservation, the shoreline is expected to retreat along the shoreface slope. This relationship has been used extensively by both researchers and managers of beaches [*Bruun*, 1983, 1988; *Larson et al.,* 1995; *Ranasinghe et al.,* 2012].

There remain criticisms on the applicability of the Bruun Rule, in some cases, through questioning of the underlying assumptions, for instance, the assumption of a depth of closure or sediment fence [*Cooper and Pilkey*, 2004; *Pilkey et al.,* 2009]. For specific applications, alongshore sediment transport gradients can locally dominate shoreline change rates such that local application of the Bruun rule may be inappropriate [e.g., *List et al.,* 1997], although *Zhang et al.* [2004] suggested the Bruun rule may be applicable away from inlets and other shoreline irregularities. Modifications of the Bruun rule to other settings such as barrier islands [*Dean and Maurmeyer*, 1983; *Larson et al.,* 1995] suggest that the long-term trajectory of shoreline retreat follows the backshore slope [*Wolinsky*, 2009], regardless of the shoreface slope. Such modified Bruun rule approaches have also been implemented in numerical models of coastal translation; these models presume a constant-shape shoreface (or relaxation about such a shape) and a fixed shoreface toe [*Stolper et al.,* 2005; *Cowell et al.,* 2006a; *Moore et al.,* 2010].

2.3. Dynamic Shoreface Evolution

The Bruun rule presumes a steady shape shoreface slope; others have used dynamic approaches to better understand shoreface dynamics and a potential origin for a dynamic equilibrium. *Dean* [1991] proposed that the shoreface attains a shape whereby the rate of wave energy dissipation becomes constant, with increasing shoreface slope for coarser sediment. Similarly, *Jenkins and Inman* [2006] applied thermodynamic principals to calculate an equilibrium profile by treating the shoreface as an "isothermal shorezone system of constant volume that dissipates wave energy." *Leont'yev* [2012] similarly used a dissipation argument where accretion and erosion are balanced by wave energy flux gradients.

Other approaches examine shoreface equilibrium through a balance of sediment transport relationships. Several models apply the energetics-based sediment transport formulations developed by *Bagnold* [1963] and adapted by *Bowen* [1980] and *Bailard* [1981]. *Stive and de Vriend* [1995] applied these energetics equations and shallow water wave assumptions in a multipanel model of lower shoreface evolution and suggest that only on geological timescales (on the order of 1000 years or more) is the bottom slope effect on sediment transport important. Similarly, *Swenson et al.* [2005] used shallow water wave assumptions and a breaking-wave closure model to investigate the basic controls on subaqueous delta progradation. Although their approach uses energetics formulations (as we do below), in this model river-supplied sediment is transported offshore by both a slope term and a presumed downwelling current with no onshore-directed fluxes. A possible concern with these previous methods is their reliance of shallow water wave assumptions rather than linear Airy wave theory as the inner shoreface to the midshelf spans intermediate water depths.

Dynamic shoreface evolution has also been studied using other sediment transport relationships such as using an empirical equations [*Patterson*, 2012]. Recent work by *Aagaard and Sørensen* [2012], computing cross-shore sediment transport based on wave orbital skewness and Longuet-Higgins' streaming velocity for the onshore components and undertow as the offshore component, argued for mainly onshore sediment transport during sea level rise. This would appear to be in contrast with the Bruun Rule, which predicts a mass transport of sediment offshore with rising sea level with a translation of the shore landward.

2.4. Outline

Here we investigate shoreface dynamics through explorations of sediment transport relationships with the following goals: (1) use relationships that can lead to a long-term steady state shoreface shape, (2) investigate the importance of linear versus shallow water waves on estimates of shoreface dynamics, and (3) quantify the order of magnitude of potential morphologic bed change as a function of depth.

From this last point, although long-term cross-shore sediment input/export to the shoreface is important for developing long-term sediment budgets [*Cowell et al.,* 2006a, 2006b], we specifically choose to pursue a definition of a morphodynamic depth of closure to describe a depth beyond which the bed shape changes slowly in response to external forcings, with a particular emphasis on changes communicated across the profile, from the shoreline to the morphodynamic depth of closure.

The paper is organized as follows: we present a theoretical approach to our formulation of shoreface evolution, including a comparison of shallow water versus linear Airy wave values. These equations lead to a steady state or dynamic equilibrium shoreface profile and, combined with the conservation of mass, lead to a formulation for shoreface evolution that takes the general form of an advection-diffusion equation describing bed evolution. Given dynamic equilibrium shoreface geometry, computation of a morphodynamic Péclet number allows us to determine the characteristic timescales of bed evolution as a function of depth, thus yielding a morphodynamic depth of shoreface closure. Finally, we compare our theoretical approach to sites estimating characteristic wave values for each site. We then discuss our findings, in particular we posit that the shoreface transition may not necessarily arise from a threshold in sediment transport, but rather because the timescales of morphologic evolution become excessively large compared to exogenous drivers, such as sea level rise.

3. Theory

In this section, we present a theoretical approach to investigate long-term shoreface evolution using an energetics-based sediment transport formulation following the approach of *Bowen* [1980]. First, we do not attempt to accurately predict sediment flux in the surf zone, which is dominated by nonlinear interactions where linear Airy wave theory and Stokes wave theory break down very quickly, and breaking waves and associated currents (such as the undertow) are present [*Madsen*, 1991; *Fredsoe and Deigaard*, 1992]. Furthermore, we ignore bedload sediment transport because suspended sediment comprises the bulk of the sediment load transported at deeper depths [*Bailard*, 1981; *Stive and de Vriend*, 1995; *Swenson et al.,* 2005], an assumption that we will justify at the end of this section. We explicitly compare shallow water wave assumptions to linear Airy wave theory because previous work has used shallow water wave assumptions, and we seek to quantitatively demonstrate the potential errors induced in understanding sediment flux and profile evolution by applying shallow water wave assumptions across the entire shoreface profile.

3.1. General Equation

Derived from *Bagnold*'s model [1963], *Bowen* [1980] developed a theoretical model for wave-driven sediment transport in the shoreface, balancing onshore-directed flows attributable to wave asymmetry and boundary layer streaming with offshore-directed slope terms. We adopt *Bowen*'s [1980] formulation for cross-shore width-averaged suspended sediment transport flux, q_s, (m^2/s)

$$q_s(z) = K\frac{u_o^3}{w_s}\left[-5u_1 - 3u_2 + \frac{\beta(x)}{w_s}u_o^2\right], \tag{1}$$

with the coefficient K (s^2/m)

$$K = \frac{16 e_s C_s \rho}{15\pi(\rho_s - \rho)\, g}, \tag{2}$$

where e_s is the suspended sediment transport efficiency factor (0.01), C_s is a bed friction factor (0.01), ρ is the seawater density (1040 kg/m^3), ρ_s is the sediment density (assumed to be quartz, 2650 kg/m^3), g is acceleration by gravity (9.81 m/s^2), β is the local bed slope, and w_s is the sediment fall velocity (m/s). Positive values are directed onshore, and negative values are directed offshore. Finally, the wave velocity components are defined by u_i ($i = 0$, 1, or 2) which represent the wave orbital velocity, Longuet-Higgins' streaming velocity, and wave asymmetry, respectively, as discussed below.

Bailard [1981] inserted an additional efficiency term (e_s) into the slope component (in addition to the constant K), which neither *Stive and de Vriend* [1995] nor we use due to the lack of a strong argument for its inclusion and deviation from the original derivation by *Bagnold* [1963]. We also choose not to nondimensionalize our formulations (as done by *Swenson et al.* [2005]), which allows us to investigate them in terms of common characteristics (i.e., wave height spanning 1–5 m and wave period spanning 6–14 s). Fall velocity is the relevant dynamic property that varies with grain size (for noncohesive sand-sized sediment), thus all references to grain size refer to variations in w_s.

3.2. Components of q_s

Here we describe the components of the sediment transport equation (1), utilizing Stokes second-order approximations of the wave contributions to sediment transport. In previous energetics approaches, both *Stive and de Vriend* [1995] and *Swenson et al.* [2005] used shallow water wave assumptions to calculate wave

velocity components, with *Swenson et al.* [2005] closing their equations using empirical breaking-wave relationships. In contrast, we calculate wave velocity components using linear theory (while offering a comparison to shallow water-wave computations). Although linear theory and shallow water assumptions converge in shallow depths approaching the surf zone, the active shoreface spans the intermediate depths where neither shallow water nor deep water wave assumptions are accurate. Note that basic equations for wave characteristics (wave height, wavelength, and wave period) can be found in the supporting information. Also note that the equations below are numbered systematically to indicate formulations derived from linear Airy wave theory (*a*) and from shallow water wave assumptions (*b*).

3.2.1. Wave Orbital Velocity: u_0

The wave orbital velocity, u_0, here the maximum bed velocity of the wave motion, represents a "stirring" term, which determines sediment concentration that can be advected by the other currents (u_1 and u_2) or moved downslope. For the wave orbital velocity, u_0 (m/s) is

$$u_0(z) = \frac{\pi H}{T \sinh(kz)} \tag{3a}$$

for linear theory and

$$u_0(z) = \frac{H g^{\frac{1}{2}}}{2 z^{\frac{1}{2}}} \tag{3b}$$

for shallow water wave assumptions, where H is the local wave height (m), T is the wave period (s), k is the wave number (m^{-1}), and z is the local water depth (m). Our choice of orbital velocity is based on the second-order Stokes derivation and time averaged. There are other numerical methods for estimating the wave orbital stirring velocity that are more accurate and can explicitly incorporate wave spectra [*Soulsby*, 2006]. However, here we use the Stokes derivation as our goal is to present an analytic formulation.

3.2.2. Streaming Velocity: u_1

The Longuet-Higgins's streaming velocity, u_1, is the mean drift approximation at the top of the wave-developed boundary layer [*Longuet-Higgins*, 1958; *Fredsoe and Deigaard*, 1992]. This net onshore-directed stress arises from asymmetrical development of the frictional boundary layer. Using linear wave theory, the streaming velocity, u_1 (m/s), can be estimated as

$$u_1(z) = \frac{3\pi^2 H^2}{4TL \sinh^2(kz)} \quad , \tag{4a}$$

and using shallow water wave assumptions

$$u_1(z) = \frac{3H^2 g^{\frac{1}{2}}}{16 z^{\frac{3}{2}}}, \tag{4b}$$

where L is the wavelength (m) [*Longuet-Higgins*, 1958].

This u_1 term could potentially specify other net flows. Within the surf zone, wave-driven setup tends to drive a net return flow at the bed, undertow [*Fredsoe and Deigaard*, 1992; *Aagaard and Sørensen*, 2012]. However, undertow rapidly dissipates outside of the surf zone, and we ignore undertow as our focus is on shoreface response. Offshore of the surf zone, wave-driven Stokes drift (and other processes) can lead to a net offshore flow. Unlike undertow in the surf zone, these shoreface return flows tend to be focused across the profile [*Lentz et al.,* 2008]. Near the bed, onshore-directed streaming stresses are expected (modeled) to be onshore, and measured flows near the bed off of North Carolina and Martha's Vineyard for profiles of ~12 m suggest onshore-directed flows near the bed [*Lentz et al.,* 2008]. On the deeper shoreface, other nonwave-driven processes such as upwelling or downwelling (as considered by *Swenson et al.* [2005]) could potentially be represented in this term. As our focus is on wave-driven transport across the shoreface, and in keeping with previous approaches, we include wave streaming as one of our onshore-directed terms along with wave asymmetry.

3.2.3. Wave Asymmetry: u_2

Wave shoaling skews wave velocities. Using Stokes second-order assumptions, these can be estimated as

$$u_2(z) = \frac{3\pi^2 H^2}{4TL \sinh^4(kz)} \tag{5a}$$

for linear theory and

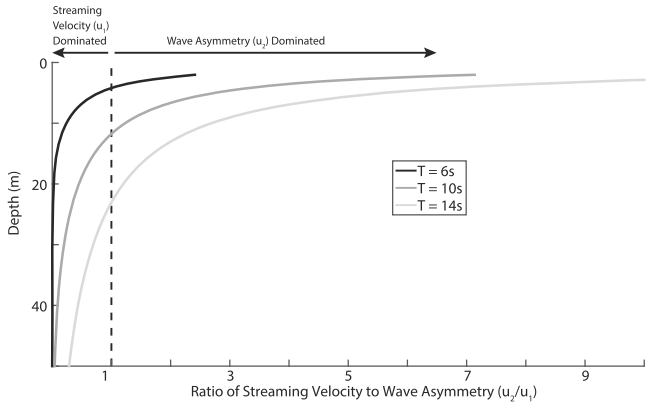

Figure 1. Ratio of cross-shore sediment flux (q_s) associated with wave asymmetry (u_2) to the cross-shore sediment flux associated with streaming velocity (u_1) over depth for varying wave period (values are independent of wave height and fall velocity).

$$u_2(z) = \frac{3H^2 g^{\frac{3}{2}} T^2}{64\pi^2 z^{\frac{5}{2}}} \tag{5b}$$

using shallow water wave assumptions [*Fredsoe and Deigaard*, 1992; *Holthuijsen*, 2007].

Our choice of wave velocity components might influence the resultant equilibrium profiles and shoreface evolution. Several recent papers have investigated the estimation of wave asymmetry velocity beyond the second-order Stokes derivation [*Abreu et al.,* 2010; *Malarkey and Davies*, 2012; *Ruessink et al.,* 2012]. In general, the Stokes second-order derivation well describes wave asymmetry velocities for depths deeper than 10–15 m [*Dean and Dalrymple*, 1991; *Holthuijsen*, 2007]. However, at very shallow depths, the wave asymmetry estimated by Stokes derivation is not a strong approximation. The relative importance of wave asymmetry is strongly dependent on wave period (Figure 1), and for shorter wave periods, wave asymmetry is only dominant in very shallow water (less than 5 m) [*Bowen*, 1980]. In very shallow water, large waves will break and strongly nonlinear wave interactions mean that linear theory is not valid. For future work, it would be interesting to investigate the impact of utilizing different wave asymmetry equations on the sediment flux equation and subsequent analysis.

3.2.4. Comparison of u_2 and u_1 Terms

The ratio of the contributions to sediment transport of the u_2 to u_1 terms is $3/5\sinh^2(kz)$ [*Stive and de Vriend*, 1995]. For typical values of wave height and wave period, sediment transport associated with the u_1 and u_2 terms tends to be of the same order of magnitude, with asymmetry (u_1) dominating in the upper profile and streaming (u_1), most important, at deeper depths (Figure 1). Increasing wave period increases the relative importance of wave asymmetry compared to wave streaming, increasing the depth at which streaming dominates. Because wave-driven undertow (or shoreface return flows) is prevalent in shallow water, these processes are less likely to affect shoreface shape as asymmetry dominates sediment flux at these shallower depths (less than 15 m). Per *Bowen's* [1980] suggestion, the use of the Stokes derivation for wave asymmetry and streaming provides insight into the relative importance of the u_1 and u_2 terms. Integrating across the profile, *Stive and de Vriend* [1995] find that about 20–30% of the sediment flux is explained by the asymmetry term, while the rest is explained by the mean terms representing the streaming term [*Rienecker and Fenton*, 1981].

3.2.5. Sediment Transport

Both the wave asymmetry and wave streaming terms direct sediment onshore, while the slope term directs sediment offshore, or downslope. Substituting the above definitions for the different order wave velocities, sediment transport for linear theory becomes

$$q_s(z) = K\frac{\pi^3 H^3}{T^3 w_s \sinh^3(kz)}\left[-\frac{15\pi^2 H^2}{4TL\sinh^2(kz)} - \frac{9\pi^2 H^2}{4TL\sinh^4(kz)} + \frac{\pi^2 H^2 \beta(x)}{w_s T^2 \sinh^2(kz)}\right] \tag{6a}$$

and

$$q_s(z) = K\frac{g^{\frac{3}{2}} H^3}{8 w_s z^{\frac{3}{2}}}\left[-\frac{15H^2 g^{\frac{1}{2}}}{16 z^{\frac{3}{2}}} - \frac{9H^2 g^{\frac{3}{2}} T^2}{64\pi^2 z^{\frac{5}{2}}} + \frac{H^2 g\beta(x)}{4 w_s z}\right] \tag{6b}$$

using shallow water wave assumptions.

Sample computations show that increasing the initial deep water wave height and wave period increases the magnitude of cross-shore sediment transport, q_s (Figure 2). Importantly, comparing the shallow water and linear theory wave assumptions, the computed values of q_s diverge increasingly with depth (Figure 2). At 50 m (for 10 s waves), the calculated cross-shore sediment transport using the shallow water assumptions is more than an order of magnitude larger than that predicted by the full linear wave theory. Even at 20 m depth, the

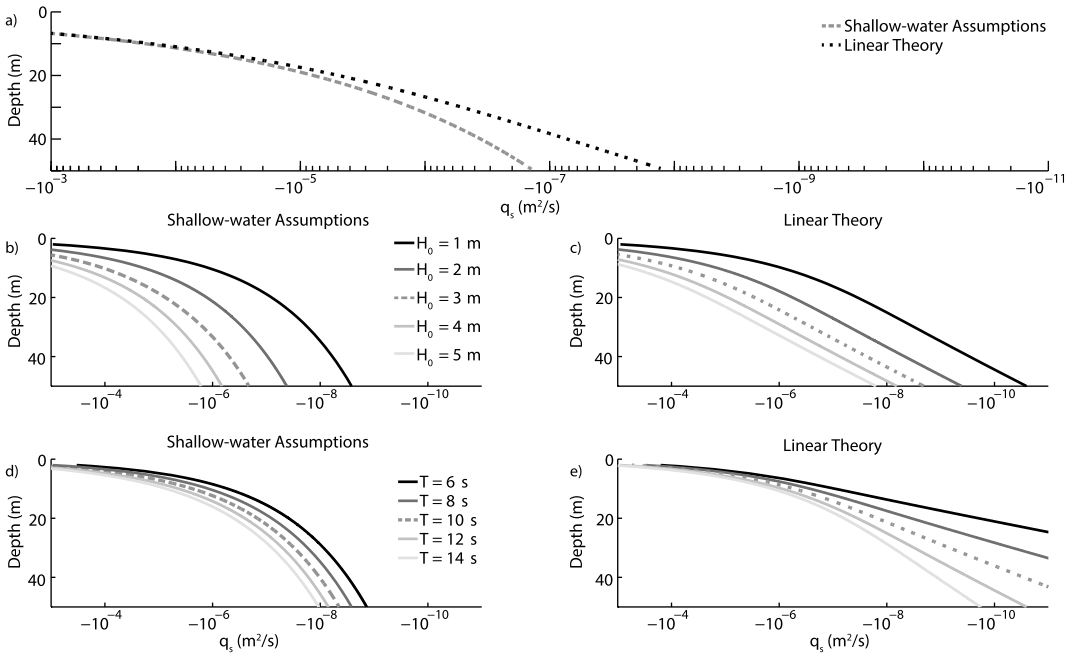

Figure 2. Plots of q_s associated with the u_1 and u_2 terms (without the slope term) over depth comparing shallow water and linear wave theory for medium-grained sand ($w_s = 0.033$ m/s) showing (a) comparison of approaches for $H_0 = 3$ m and $T = 10$ s and values for varying (b and c) deep water wave heights and (d and e) period with negative values indicating onshore-directed sediment transport.

shallow water wave assumptions predict a cross-shore sediment transport ~3 times more. The negative values of q_s indicate onshore-directed sediment transport when the slope term is ignored.

3.3. Equilibrium Profile

Following the approach of *Bowen* [1980], we use the formulation for shoreface sediment transport to derive a steady state, dynamic equilibrium profile by balancing the onshore-directed terms (streaming and asymmetry) with the offshore-directed slope term. For a long-term zero-flux condition, i.e., $q_s = 0$, it is then possible to solve for an equilibrium slope and equilibrium profile such that

$$\beta_0(z) = \frac{w_s}{u_0^2}[5u_1 + 3u_2]. \tag{7}$$

Equilibrium slopes can be computed for linear wave theory

$$\beta_0(z) = \frac{3w_s T}{4L}\left[5 + \frac{3}{\sinh^2(kz)}\right] \tag{7a}$$

and shallow water wave assumptions

$$\beta_0(z) = \frac{3w_s}{4z^{\frac{1}{2}}g^{\frac{1}{2}}}\left[5 + \frac{3gT^2}{4\pi^2 z}\right]. \tag{7b}$$

Note that, in both cases, the dynamic equilibrium slope has no dependence on wave height and instead only depends on the wavelength, wave period, and sediment fall velocity.

Equations (7a) and (7b) are not conducive to analytical integration; however, equilibrium profiles can be numerically integrated from the shoreline. Using first-order Eulerian integration starting from the shoreline (starting at 2 m depth to avoid integration of infinite slopes), computed equilibrium profiles for typical wave conditions show little difference in shoreface shape for shallow water wave assumptions and linear theory (Figure 3). Spanning fall velocities ranging from 0.008 to 0.16 m/s, corresponding to grain size ranging from very fine to coarse sand (0.01–1 mm), the strongest control on equilibrium profile slope is the grain size

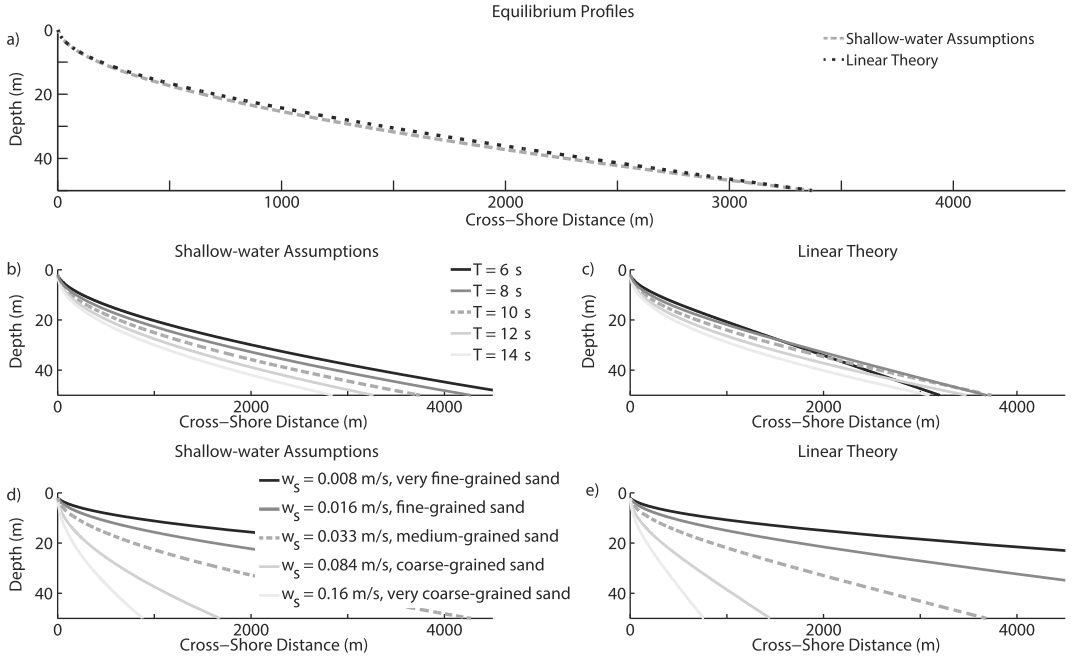

Figure 3. Computed equilibrium profiles (a) comparing shallow water and linear wave theory for $T = 10$ s and $w_s = 0.033$ m/s for varying (b and c) wave period and (d and e) fall velocity.

(sediment fall velocity) [*Fredsoe and Deigaard*, 1992]. Our choice of Stokes derivation for u_2 is not the best option in shallow water, which potentially does affect the shape of the upper profile.

Below, we will make more explicit comparisons between measured and computed equilibrium profiles. *Dean*'s [1991] equilibrium profiles, derived for the surf zone, are monotonic and dependent on grain size, and assuming constant wave energy dissipation, are much less steep with slopes at least an order of magnitude less. The profile dimensions predicted by our approach (equation (7)) match those of natural shorefaces with a convex shape. We cannot, however, exactly compare equilibrium profiles as the Dean profiles are empirical or calibrated forms and are in particular applied to shallower portions of the profile (often the top 5 m or less). As *Bowen* [1980] found, our equilibrium profile equation is a first-order approximation of a complex system in which grain size seems to have the strongest control (Figure 3).

Bailard's [1981] formulation for suspended sediment transport multiplies the slope term again by the efficiency term, e_s. Inclusion of this additional efficiency parameter would predict equilibrium shoreface profiles over an order of magnitude (~40 times) flatter. For this same reason, *Stive and de Vriend* [1995] argue against the inclusion of this term; accordingly, we also do not use the extra efficiency factor introduced by *Bailard* [1981], instead we follow *Bagnold*'s [1963] original derivation.

3.4. Exner Equation

A shoreface bed evolution formulation can be derived by combining equation (1) with the conservation of sediment mass through the application of the Exner equation relating bed evolution to the divergence of sediment flux, similar to *Swenson et al.* [2005]. Combining equation (1) for cross-shore sediment flux with the Exner equation

$$\frac{\partial z}{\partial t} = \frac{1}{\varepsilon_o}\frac{\partial q_s}{\partial x} \tag{8}$$

where ε_o is one minus the porosity and using the chain rule

$$\frac{\partial q_s}{\partial x} = \frac{\partial q}{\partial z}\cdot\frac{\partial z}{\partial x} \tag{9}$$

yields

$$\frac{\partial z}{\partial t} = K\frac{u_o^2}{\varepsilon_o w_s}\left[\left(-5u_1' u_0 - 15u_o' u_1 - 3u_2' u_0 - 9u_0' u_2 + \frac{5\beta_0}{w_s}u_0' u_0^2\right)\frac{\partial z}{\partial x} + \left(\frac{u_0^3}{w_s}\right)\frac{\partial^2 z}{\partial x^2}\right]. \tag{10}$$

The single prime above the wave velocity components represents the derivative relative to depth, z (the values of these derivatives can be found in the supporting information).

The general form of equation (10) is an advection-diffusion equation of the form

$$\frac{\partial z}{\partial t} = \left[(V)\frac{\partial z}{\partial x} + (D)\frac{\partial^2 z}{\partial x^2}\right]. \tag{11}$$

The advection term, V (m/s), represents the kinematic celerity for bed evolution (m/s)

$$V(z) = K\frac{u_o^2}{\varepsilon_o w_s}V_c \tag{12}$$

with the advection coefficient, V_c, (m/s^2)

$$V_c(z) = -5u_1' u_0 - 15u_o' u_1 - 3u_2' u_0 - 9u_0' u_2 + \frac{5\beta_0}{w_s}u_0' u_0^2. \tag{13}$$

The diffusivity (m^2/s) is

$$D(z) = K\frac{u_o^2}{\varepsilon_o w_s}D_c \tag{14}$$

with the diffusivity coefficient, D_c, (m^2/s^2)

$$D_c(z) = \frac{u_o^3}{w_s}. \tag{15}$$

Using linear wave theory, the diffusivity equals

$$D(z) = K\frac{\pi^5 H^5}{\varepsilon_o w_s^2 T^5 \sinh^5(kz)}. \tag{16}$$

3.5. Morphodynamic Péclet Number

Advection-diffusion equations can be characterized using the nondimensional Péclet number, commonly applied to fluid flows, which quantifies the relative influence of advection versus diffusion in transport phenomena for a given system. Estimation of morphodynamic Péclet numbers has seen recent interest in terrestrial geomorphology [*Perron et al.,* 2008; *Pritchard et al.,* 2009; *Pelletier and Perron*, 2012]. Here we adapt the concept of a morphodynamic Péclet number to describe coastal profile evolution.

The Péclet number is defined as

$$Pe = \frac{Vl}{D}\ , \tag{17}$$

where $Pe > 1$ characterizes an advection-dominated system and $Pe < 1$ characterizes a diffusion-dominated system. Dominance in this case refers to the faster process that controls system evolution. To compute a Péclet number for our problem, we require a characteristic length scale (l), and we choose the steady state profile distance to the coast, x_{eq}. We select this distance as it scales how the bed may respond to a change of the shoreline (or vice versa). Using the kinematic celerity, V (equation (12)), and the diffusivity, D (equation (14)), the morphodynamic, depth-dependent Péclet number (equation (17)) for an equilibrium shoreface then becomes

$$Pe(z) = \frac{V_c x_{eq} w_s}{u_0^3}. \tag{18}$$

Both the shallow water and linear theory computations of the Péclet number predict a diffusively dominated system (Figure 4). As the morphodynamic Péclet number is a ratio of the advection coefficient (V_c, equation (13)) and a power of the stirring term, $u_0{}^3$, we see that this advection coefficient reduces more rapidly with depth than the stirring term influence, thus decreasing the Péclet number at deeper depths.

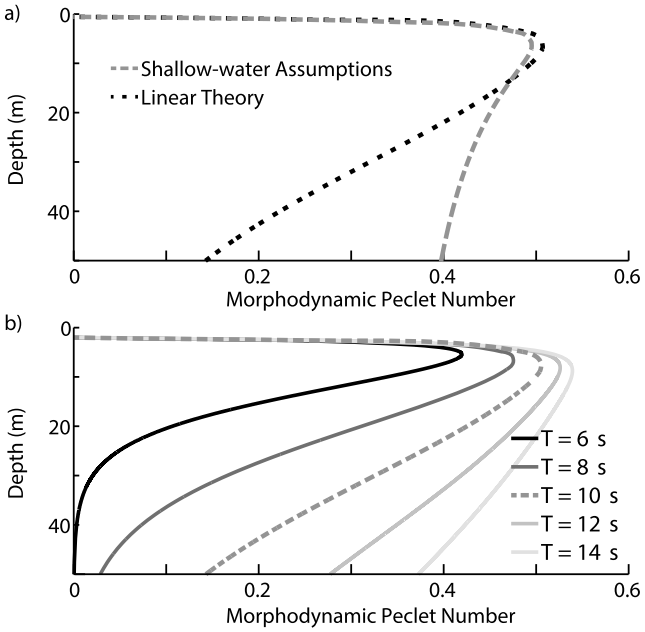

Figure 4. Morphodynamic Péclet number of an equilibrium shoreface over depth (a) comparing linear theory and shallow water wave assumptions for $H_0 = 3$ m and $T = 10$ s. (b) Péclet number for varying wave period over depth using linear wave theory for $H_0 = 3$ m.

Numerically computed morphodynamic Péclet numbers show only a dependence on wave period and not wave height or settling velocity (Figure 4). Although there may be an expected dependence on grain size, the equilibrium cross-shore distance, x_{eq}, integrates the equilibrium slope, β_0 (equation (7)), which has in inverse dependence on grain size, w_s^{-1}. Therefore, the computed morphodynamic Péclet number is unaffected by grain size. On the other hand, increasing the wave period increases the importance of the wave asymmetry in the advection term.

3.6. Characteristic Timescales of Shoreface Evolution

By demonstrating that slope-based diffusivity dominates profile evolution, the morphodynamic Péclet analysis allows us to calculate a depth-dependent characteristic timescale of shoreface evolution. Dimensionally, this timescale can be defined as

$$T_{\text{diff}} = \frac{l^2}{D} \tag{19}$$

where l is a characteristic length scale (again taken to be the distance to the steady state shoreline, x_{eq}) and D is the diffusivity (equation (14)). The length scale represents the width of the shoreface, such that any response must be transmitted from the onshore to the offshore limits. The morphodynamic Péclet analysis is essentially a ratio of the characteristic timescales of advection versus diffusion, with the faster process setting the timescale needed for the system to trend toward a near steady state.

The diffusional timescale for shoreface evolution then becomes

$$T_{\text{diff}}(z) = \frac{x_{\text{eq}}^2 w_s^2}{K\varepsilon_o u_0^5} \quad . \tag{20}$$

Substituting the terms from linear theory yields

$$T_{\text{diff}}(z) = \frac{x_{\text{eq}}^2 w_s^2 \mathrm{T}^5 \sinh^5(kz)}{K\varepsilon_o \pi^5 H^5}. \tag{20a}$$

Similar to the morphodynamic Péclet number (equation (18)), there is no dependence on grain size as x_{eq} has an inverse dependence on w_s (equation (7))—the first two terms cancel out. Accordingly, the depth-dependent characteristic diffusive timescale varies primarily with deep water wave height and wave period (Figure 5) and, at equilibrium configurations, perhaps surprisingly does not depend on grain size.

For typical values of deep water wave height and wave period, shoreface response timescales become significantly large (>1000 years) at depths between 10 and 30 m, suggesting a type of morphodynamic depth of closure (MDOC). In other words, profile evolution and, in particular, sediment transport may continue beyond this depth, but evolution of the shoreface shape becomes geologically slow and the bed shape response to environmental changes becomes virtually nonexistent. The equilibrium profile is affected by our choice of wave asymmetry, but the MDOC estimates are not controlled by either our choice of wave asymmetry or streaming.

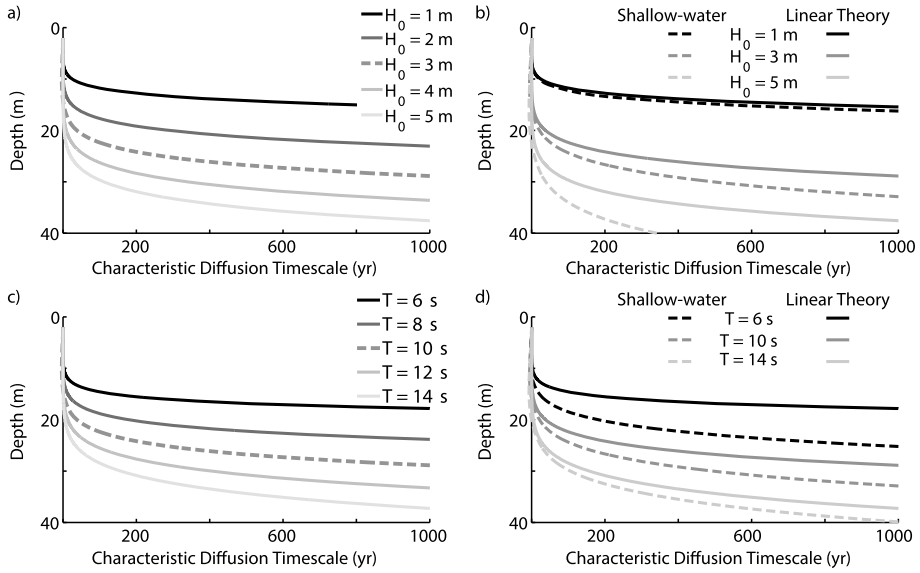

Figure 5. Computed characteristic timescale of diffusion using linear theory over depth with varying (a) deep water wave height with $T = 10$ s and (c) varying wave period with $H_0 = 3$ m. Comparison of linear theory to shallow water assumptions with varying (b) wave height with $T = 10$ s and with varying (d) wave period with $H_0 = 3$ m.

The same analysis can be used to calculate a timescale of kinematic celerity (Figure S4). Because the morphodynamic Péclet number predicts a diffusively dominated shoreface, the timescale of kinematic celerity systematically predicts shallower MDOC than using the timescale of diffusivity and decreased shoreface activity. The slower process predicts a less active shoreface, and therefore a shallower closure depth. However, because the Péclet numbers are close to unity, advection and diffusion timescales are almost the same, and the MDOC predicted using either the timescale of diffusivity or of kinematic celerity are within 2–5 m of each other at the 1000 year timescale.

The computed morphodynamic depth of closure increases with increasing wave height and increasing wave period (Figure 6). Increasing wave height increases orbital velocities, and increasing wave period deepens bed interaction (as expected from previous equations). Sediment grain size should not affect the response time or closure depth, only the equilibrium shoreface shape itself. In general, increasing response time by an order of magnitude (from 10 to 100 years) tends to increase the closure depth predicted by linear Airy wave theory by approximately 5 m.

Note that shallow water wave assumptions predict far more active shorefaces than those predicted by linear waves, particularly for larger wave heights (Figures 5b and 4d), suggesting a deeper morphodynamic depth of closure than linear wave theory. Furthermore, linear Airy wave theory predicts a more tightly constrained shoreface transition than shallow water wave theory—a strongly defined effective wave base across only a few meters of depth change. As such, linear wave theory suggests only a few meters difference in depth of the MDOC for the 100 and 1000 year timescales, which suggests that, geologically, there is a rather tightly constrained MDOC. On the other hand, shallow water wave assumptions do not show such a strong break in process rate across depth; as these assumptions are applied at ~20 m depths, shallow water waves might suggest a more indistinct shoreface transition than is appropriate.

3.7. Discussion of the Theoretical Approach

Here we discuss some of the assumptions and implications of the theoretical model of shoreface evolution. First, we address the assumption that bedload transport dominates on the shoreface and then discuss the influence of offshore decreases in grain size. We then discuss the mechanistic response of an equilibrium shoreface to sea level rise.

3.7.1. Suspended Versus Bedload Transport

Our analysis assumes that suspended sediment transport dominates on the middle and lower shoreface, an assumption that needs to be justified as bedload transport occurs throughout the shoreface [*Kleinhans*, 2002].

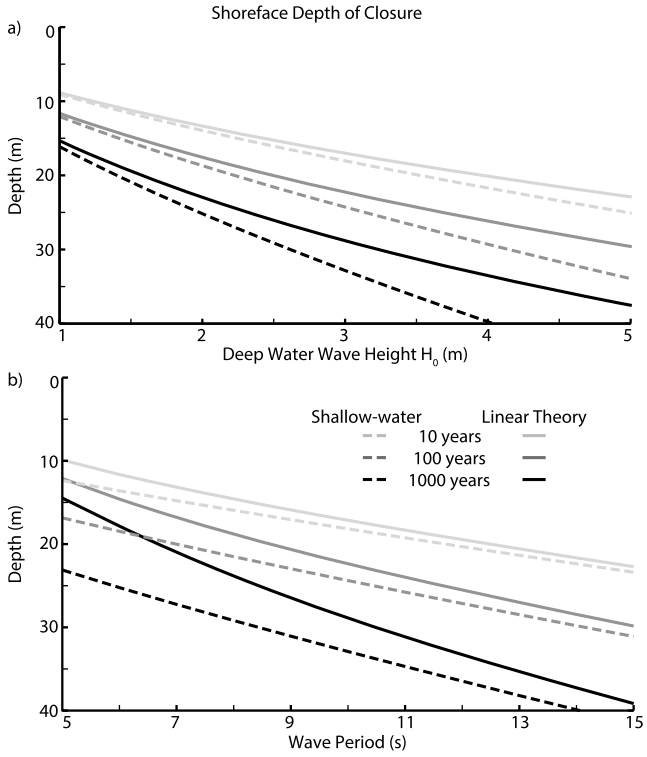

Figure 6. Computed morphodynamic closure depths using shallow water wave assumptions (dashed lines) and linear theory (solid lines) for (a) varying deep water wave height (with $T = 10$ s) and (b) varying wave period (with $H_0 = 3$ m).

Bowen [1980] and *Stive and de Vriend* [1995] demonstrate that the ratio between suspended sediment load and bedload transport for energetics approaches can be approximated as ~1/15 u_0/w_s. For values of this ratio greater than unity, the magnitude of suspended sediment transport exceeds the magnitude of bedload sediment transport. This suspended versus bedload transport ratio varies with grain size (sediment fall velocity), such that the smaller the grain size, the more likely it is carried in suspension.

For small wave heights (e.g., $H_0 = 1$ m), bedload does indeed tend to dominate transport across the shoreface. However, as we present in the next section and also demonstrated by *Stive and de Vriend* [1995], effective wave heights for shoreface evolution tend to be much larger due to the weighting of sediment transport by $H_s^5 T^{-5} \sinh^{-5}(kz)$. Sample computations for a characteristic morphologic wave height ($H_0 = 5$ m) and wave period ($T = 9$ s) similar to those computed for our representative coastal locations show that suspended sediment transport dominates over shallow depths (<10 m) for coarse sand and over the entire shoreface for finer-grained sediment (Figure 7). During morphologically important conditions, the entire shelf is mobilized as suspended sediment. Given the general trend of fining of sediments with increasing offshore distance [*Zenkovitch*, 1946], suspended sediment transport should be the most effective long-term process across the entire shoreface as is often assumed [*Kleinhans*, 2002]. Moreover, for our specific study sites, suspended sediment flux is an order of magnitude larger than bedload sediment flux for medium-grained sand (Figure S1 in the supporting information).

Furthermore, Figure 7 assumes that the same characteristic wave height and wave period (morphodynamic characteristic wave conditions) are used for bedload and suspended load transport. If the diffusivity equation (16) is investigated, suspended load is weighted by u_0^5 (hence the new weighting on $H_0^5 T^{-5} \sinh^{-5}(kz)$) while bedload should be weighted by u_0^3 [*Bagnold*, 1963]. This separate weighting for bedload was used to calculate the H_{0b} and T_b (Figure S1) with the result that the morphodynamically important wave values are smaller for bedload than for suspended load. Figure 7, however, does not vary these values; given the above analysis, suspended load dominates even greater than shown in the ratio.

3.7.2. Offshore Fining

In general, the computed equilibrium profiles and analysis above assume a constant sediment size across the profile. Again, this is typically not the case for natural shorefaces where sediment tends to fine offshore. However, offshore fining is not incongruous with our approach for the following two reasons. First, our approach defines an equilibrium slope as a function of depth (equation (7)). If shorefaces fine with depth, this would suggest "compound" shoreface slopes with local slopes defined by the local sediment characteristics (with local sediment distributions affected by both transport processes and, more importantly, local sediment availability). Second, as we discuss above, grain size effects cancel out when computing characteristic timescales, such that grain size only affects profile shape and profile diffusivity. Also, offshore fining of sediment increases the importance of suspended load transport on the deeper profile as the finer the sediment the more is transported as suspended load versus bedload, all other things being held equal.

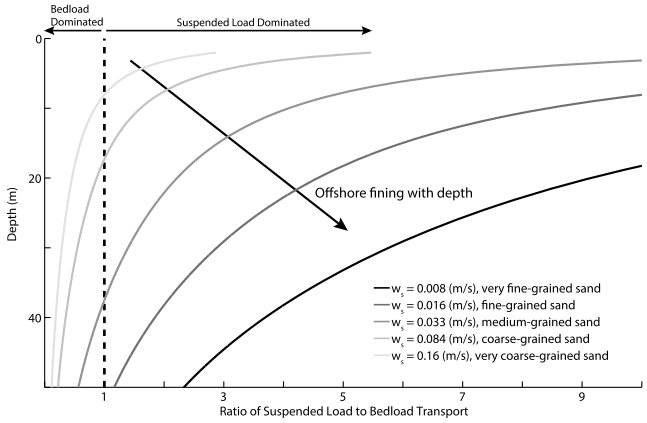

Figure 7. Ratio of suspended load to bedload transport over depth for $H_0 = 5$ m and $T = 9$ s for varying fall velocity.

3.7.3. Sea Level Rise Response of Equilibrium Profiles

The analysis provided here potentially reconciles several apparent paradoxes regarding shoreface response to sea level rise. For our formulation, if sea level rises instantaneously, both the onshore- and offshore-directed terms will be reduced. However, the reduction in the onshore terms is greater than the reduction in the offshore term—the shoreface is oversteepened and sediment would consequently be transferred offshore in the manner suggested by the Bruun Rule (Figure 8). Note that the magnitude of wave asymmetry (u_2) is decreased more than wave streaming (u_1) for driving sediment onshore with the instantaneous increase of sea level (Figure 8b).

On the other hand, if sediment is removed from the shoreface, perhaps by onshore-directed fluxes such as overwash [*Ashton and Ortiz*, 2011; *Lorenzo-Trueba and Ashton*, 2014] or aeolian processes [*Davidson-Arnott*, 2005], this will result in an overall flattening of the profile, reducing the offshore-directed slope-driven sediment transport, resulting in net onshore sediment transport. Likewise, aggradation of sediment in the upper shoreface, perhaps due to positive alongshore sediment transport gradients, would oversteepen the shoreface profile, leading to offshore transport within the active morphological shoreface. Short-term changes of the profile merely redistribute the mass across the profile, rather than changing the total shoreface volume.

Our approach can also provide insight into the findings from other process-based investigations of shoreface evolution. Recently, *Aagaard and Sørensen* [2012] used a model of shoreface sediment transport including two onshore-directed terms based upon streaming and asymmetry (skewness), similar to those used in our analysis (u_1 and u_2, respectively). Applying their model to a synthetic Dean-type profile, they concluded that sea level rise should drive sediment flux onshore. However, close inspection of their results (*Aagaard and Sørensen* [2012] in Figures 6 and 7) suggests that their synthetic input profile is not in dynamic equilibrium for the initial case of an unperturbed sea level. Their model then suggests that a raised sea level reduces the onshore component of sediment transport offshore of the surf zone (Figure 8). If a dynamic equilibrium existed for *Aagaard and Sørensen*'s [2012] synthetic shoreface shape, a reduction in onshore sediment transport should result in an offshore-directed flux. Therefore, their model results appear to be congruent with our results and the concepts underlying the Bruun Rule

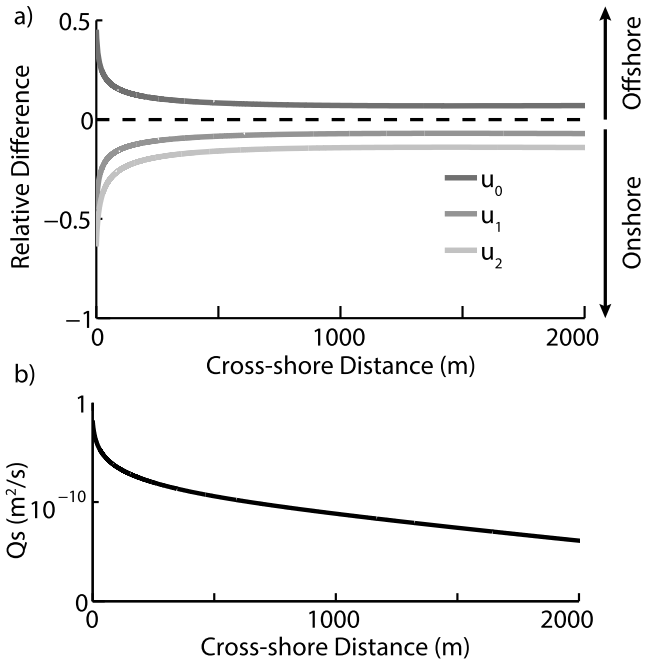

Figure 8. Computed effect of 1 m of sea level rise on an equilibrium profile of $w_s = 0.033$ m/s using linear theory on (a) components of cross-shore sediment transport and (b) total cross-shore sediment transport (positive direction is offshore) for $H_0 = 3$ m and $T = 10$ s.

which suggest that sea level rise, by reducing onshore transport, oversteepens shoreface profiles, driving a net seaward flux; their interpretation of onshore-directed flux appears to conflict with their results.

As we state above, *Swenson et al.* [2005] (and also *Hutton and Syvitski* [2008]) applied a similar energetics model to clinoform development, using only offshore-directed terms: a slope-based term and a downwelling velocity. As their models [*Swenson et al.,* 2005; *Hutton and Syvitski*, 2008] contain no onshore-directed components of flux, true dynamic profile equilibrium cannot exist. Although these applications may be appropriate for actively prograding deltas, the development of a dynamic equilibrium profile is a necessary requirement for coastal features, such as barrier islands, to survive on a passive coast.

4. Application

Although the formulations above use a single set of wave characteristics (height and period), at any given location these driving forces are constantly changing—fluctuating between calm and storm conditions. For a given location and associated wave climate, what are the characteristic wave conditions affecting profile evolution? Are they the wave heights and periods that occur most frequently (the mean wave climate), or are they storm waves (the extreme events)? Should conditions be selected based upon a set return interval or in some way weighted by sediment transport processes? We approach this problem by utilizing the classic geomorphic approach of *Wolman and Miller* [1960], which weights an event's frequency by the amount of potential morphologic change. Adopting this frequency-magnitude approach [*Wolman and Miller*, 1960; *Wolman and Gerson*, 1978; *Brunsden and Thornes*, 1979; *Sullivan and Lucas*, 2007] to address shoreface evolution, we weight wave conditions based upon the capacity for sediment transport (instead of wave energy density, i.e., H^2, alone as used by *Jimenez and Sanchez-Arcilla* [2004] and *Peters and Loss* [2012]). We apply our theoretical formulation of shoreface evolution to six sites by calculating average profiles for each location and comparing these to estimated equilibrium profiles while also predicting a characteristic diffusive timescale across each profile.

4.1. Analysis Sites and Data

We select six sites along the U.S. coast that span a range of oceanographic and geologic conditions to compare with our model: Eel River, CA, Martha's Vineyard, MA, Fire Island, NY, Santa Rosa Island, FL, Duck Pier, NC, and Onslow Bay, NC (Figure 9). We chose sites from both active margin (Eel River, CA) and passive margins (Martha's Vineyard, MA, Fire Island, NY, Duck Pier, NC, and Onslow Bay, NC). In addition, we choose sites from different ocean basins (Atlantic Ocean, Pacific Ocean, and the Gulf of Mexico) to explore a variety of wave climates.

For each site, we use the Wave Information Studies (WIS) array of virtual buoys representing a data set of long-term (20 years) hindcasted wave data [*Jensen*, 2010] every 3 h from 1980 to 1999 (Figure 9). Additionally, we compute an average profile for each coast by averaging cross-shore profiles from GeoMapApp™ bathymetric data [*Haxby*, 2012] and the NASA Aster-USGS basemap [*Ministry of Economy, Trade, and Industry and National Aeronautics and Space Administration*, 2011], where offshore distance was calculated relative to the location of zero elevation from WGS84. The profiles are averaged together and smoothed.

4.1.1. Wave Data Analysis

For each site, virtual WIS buoy data are analyzed and weighted to calculate a representative wave height and wave period. The virtual WIS buoy locations are typically deeper than 20 m, but to ensure consistency among all the sites, waves from the WIS buoys are back-shoaled to deep water ($z/L_0 > 0.5$) values. Computed deep water values are within 10% of the nonback-shoaled values.

For both linear Airy wave theory (equation (6a)) and shallow water assumptions (equation (6b)), the cross-shore sediment flux is weighted by wave orbital velocity (u_0) to the fifth power ($q_s \propto {u_0}^5 \propto {H_s}^5 T^{-5} \sinh^{-5}(kz)$) (equations (1) and (3a)). Similarly, the magnitude of the diffusivity term (equation (14)), describing bed evolution, is also dependent on wave orbital velocity (u_0) to the fifth power. The potential contributions to sediment transport for given wave conditions should be weighted accordingly (Figure 10); the means of these weighted distributions therefore represent the morphodynamically average wave conditions. By weighting the wave height and wave period according to the diffusivity (equation (16)), we use the center of mass of the two-dimensional histogram of weighted wave height and wave period shoaled to a depth of 30 m for

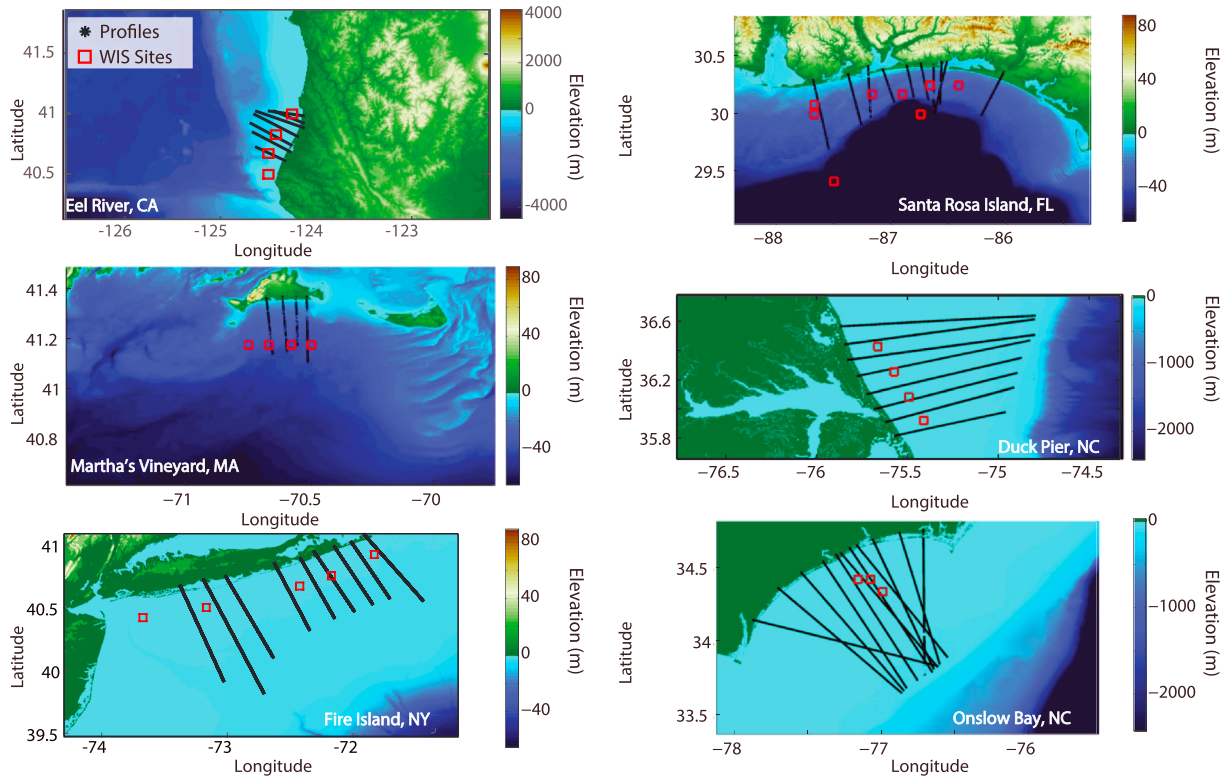

Figure 9. The six analysis locations showing bathymetric data, topographic data, extracted shelf profiles, and the location of the virtual WIS buoys.

every study site as the morphodynamically important wave conditions. Wave period scales linearly with wave height for our sites, and weighting the two-dimensional histogram by wave period and sinh(*kz*) to the negative fifth power does not have a large impact on the estimated characteristic wave conditions (less than 10%) compared to just weighting by wave height to the fifth power. At first order, wave height to the fifth power has the strongest control on estimating the characteristic wave conditions.

Using these wave height and period calculations, we are able to estimate the characteristic morphodynamic wave conditions for each site (Figure 10). Weighting wave influence by potential contributions to cross-shore sediment transport ($q_s \propto u_0^5$) emphasizes the importance of extreme wave events, the tail of the distribution (Figure 10). Thus, using the unweighted or mean wave conditions as representative of the sediment transport mechanisms would systematically underestimate the characteristic morphodynamic wave conditions. This strong influence of large wave events on shoreface evolution also suggests that the omission of threshold sediment entrainment in our formulations does not have a morphological significance.

4.2. Profile Comparisons

Using the morphodynamically representative wave characteristics (wave period and wave height), we can compute estimated morphodynamic depths of closure for measured profiles by calculating the timescale of diffusion (equation (20a)). Our first comparison is for the Eel River, CA, which has been previously studied by *Friedrichs and Wright* [2004] to test their model of wave-suspended cross-shelf gravity flows (Figure 11). While their model performs well in predicting the convexity of the deeper shelf from 40 to 130 m, the fit and trend do not match for shallower depths where the shoreface becomes concave (Figure 4) [*Friedrichs and Wright*, 2004]. Predicted equilibrium slopes and morphodynamic closure depths from our model provide a better match to slopes and trends across inner to midshelf depths (5–40 m) (Figure 11). As our model nears predicted shoreface closure depths, concavity dovetails into the convex slopes predicted by their model, suggesting a transition in process across depth. Our model bridges the gap between their model and shallower depths (Figure 11).

Comparisons of predicted closure depths for passive margins present more of a mixed bag (Figures 12 and 13). In some cases, the calculated morphodynamic depth of closure at 100 or 1000 years visually coincides

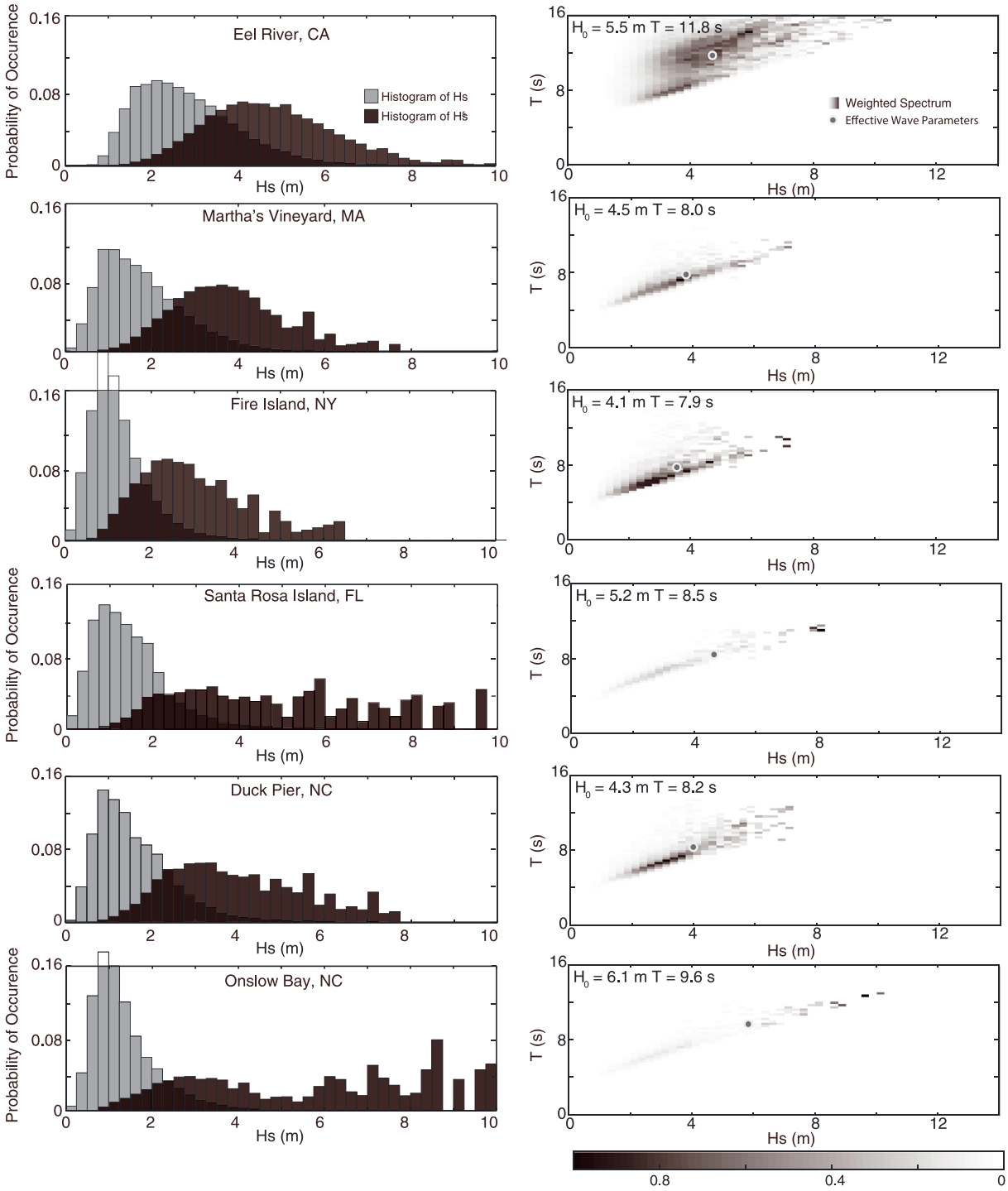

Figure 10. Wave event analysis for the 20 year hindcasted data set, plotting (left column) probability distribution functions of the wave height weighted by the mean wave height (H, grey) and H^5 (black) and (right column) the normalized two-dimensional histogram of wave height and wave period weighted by $H^5T^{-5}\sinh^{-5}(kz)$ at 30 m depth, with the center of mass of the 2-D histogram denoted by the grey filled circle used in calculating the characteristic morphodynamic wave height and wave period.

with the offshore break in slope from the steeper shoreface to the shelf (Figure 12). In other cases, the fit is not strong, and the Onslow Bay, NC, site stands out as a poor fit. For Onslow Bay, this likely demonstrates a strong geologic control of the shoreface morphology; such control has been suggested previously by field work at nearby Wrightsville Beach, NC [*Thieler et al.,* 1995, 2001].

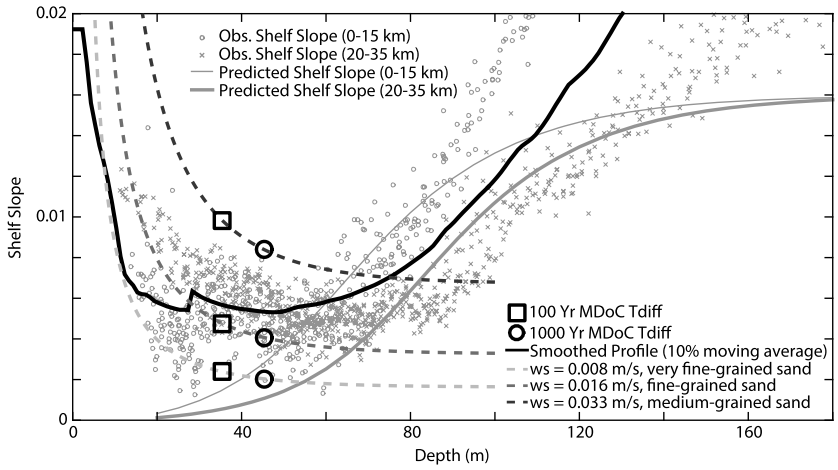

Figure 11. For Eel River, CA, comparison of measured slopes with predicted equilibrium shoreface slopes (dash lines) and computed morphodynamic depth of closure to predicted equilibrium shelf slopes adapted after *Friedrichs and Wright* [2004, Figure 4].

As a further comparison, we compute theoretical steady state slopes (equation (7)) using the representative wave height and wave period at each site for different grain sizes (from coarse to very fine-grained sand) and corresponding depths of closure (Figure 13). Computed equilibrium slopes for weighted wave conditions reasonably match the measured slopes above the computed closure depths. Slopes at shallow depths (<5 m) are in poor agreement. This is expected as surf zone processes dominate at these depths (also the

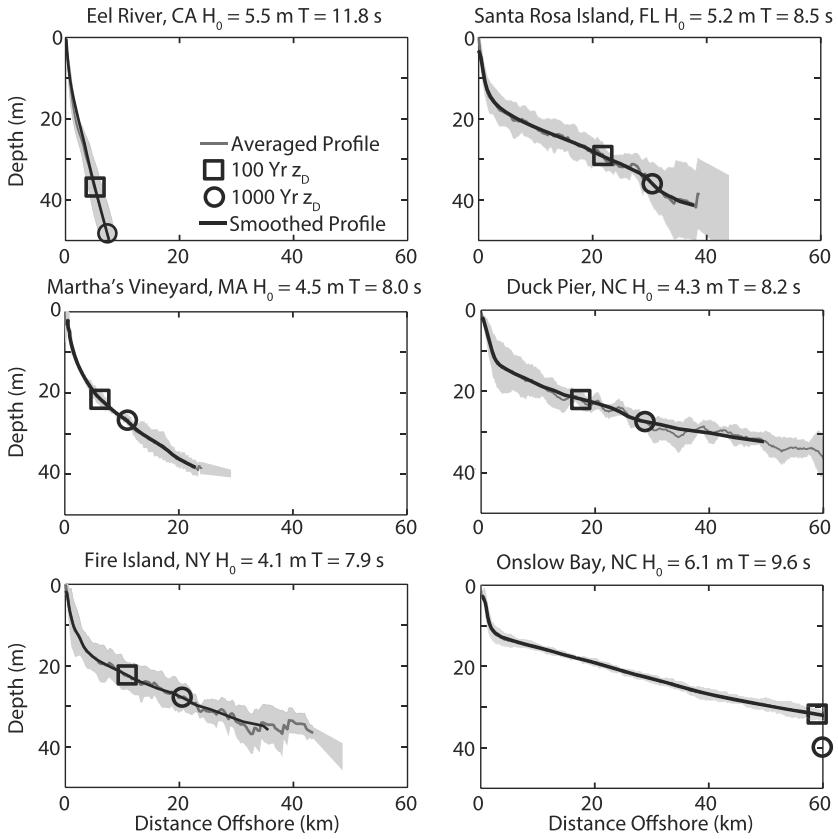

Figure 12. Averaged (grey line) and smoothed (black line) profiles with standard deviation of profiles indicated by grey shading for six sites with markers indicating the computed morphodynamic depth of closure for characteristic diffusion timescales at 100 years and 1000 years (z_D).

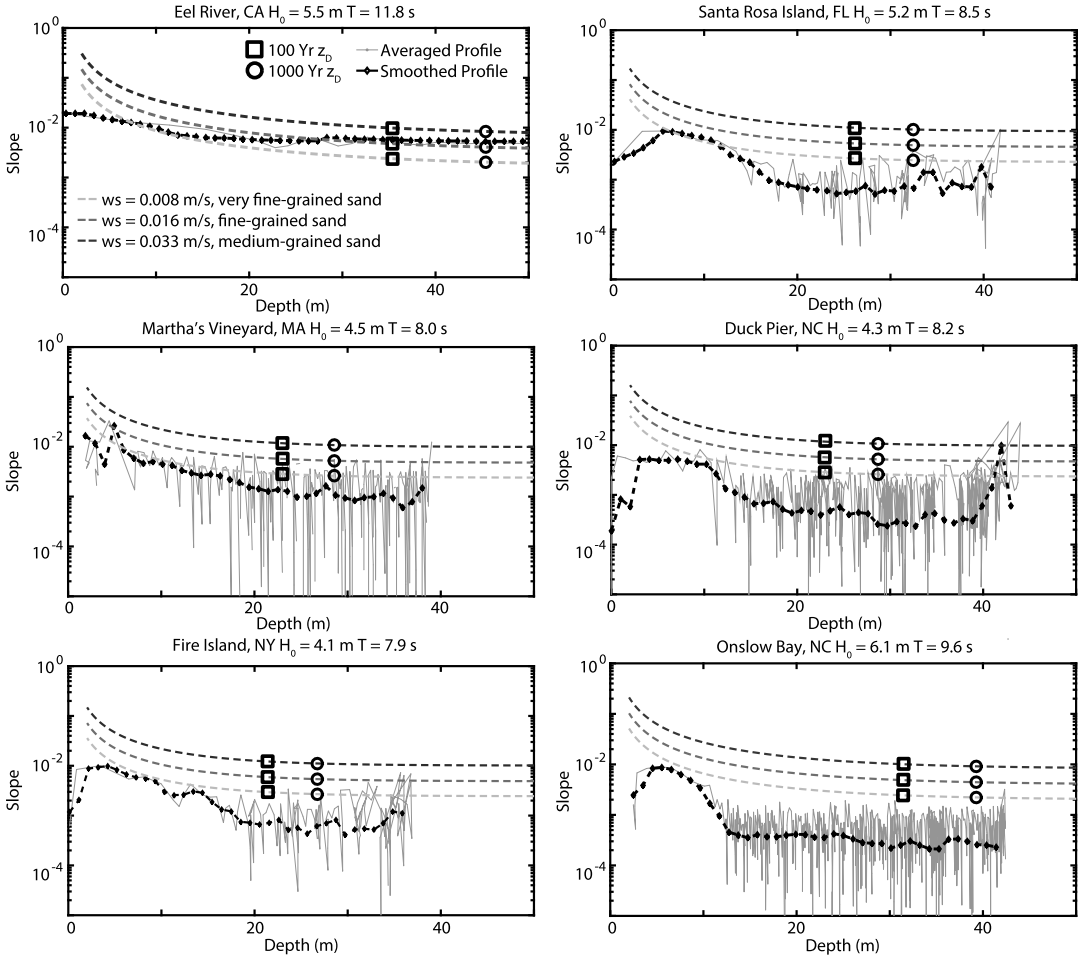

Figure 13. Derivative of computed steady state profiles with varying fall velocities compared with smoothed averaged profiles for six study sites. Included are computed morphodynamic depth of closure values for characteristic diffusion timescales at 100 years and 1000 years.

bathymetric data are less accurate close to shore), and our model is not intended to be used in the surf zone. We also note that our sediment transport formulation is uncalibrated, in contrast to other approaches based upon empirical (or semiempirical) fits.

At all sites, the general trend is a flattening of the shoreface slope with increasing depth with the exception of the active margin location, the mouth of the Eel River, where the slope eventually begins to steepen with depth as discussed above. A reduction in slope for the smoothed profiles typically is apparent around 20–25 m depth (Figure 13). This depth tends to correspond with the predicted morphodynamic depth of closure from 100 to year or 1000 year timescales of diffusivity (within 5 m). Even within the active shoreface region, the predicted equilibrium slopes tend to be steeper than smoothed actual slopes for all sites except the Eel River, CA (Figure 13). Actual profiles also decrease in slope faster than profiles computed for single grain sizes; offshore sediment fining typical of most shorefaces could be responsible for this rapid slope decrease. Martha's Vineyard, MA, and Fire Island, NY, which share similar wave climates and geologic settings, also have similar profile shapes and are among the better matches to our model predictions.

We then compare our approach to traditional methods for computing closure depth using the *Hallermeier* [1978] and *Birkemeier* [1985] equations. Utilizing the WIS virtual buoys for each site, we calculate the closure depth using these methods for each year of data using the 12 h exceedance. Averaging these values at each site, we interpret these as 1 year closure depths. We also estimate a 20 year closure depth from the 12 h exceedance from the entire data series (all 20 years). These computed closure depths are all shallower than the morphodynamic closure depths estimated using our method (which are continuous functions of time interval) (Figure 14) [*Hallermeier*, 1978; *Nicholls et al.,* 1996, 1998]. However, the disagreement between the

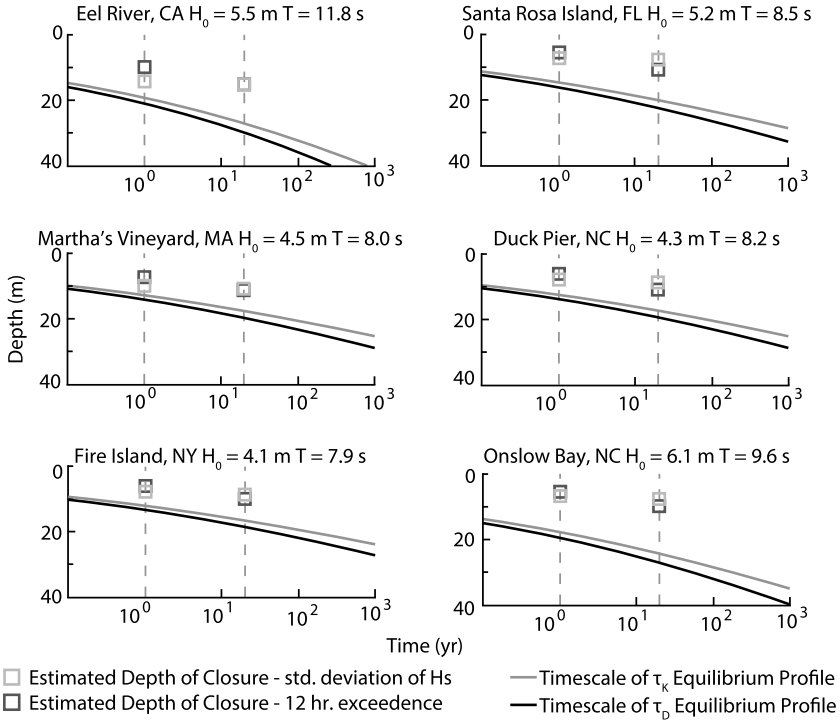

Figure 14. Theoretical computations of characteristic timescales of diffusion and kinematic celerity using linear theory compared to computations of depth of closure using *Hallermeier* [1978] and *Birkemeier* [1985] for 1 year and 20 years for six field locations and $w_s = 0.033$ m/s.

methods interpreting the Hallermeier and Birkemeier methods as 1 year closure depths is not as large as would be presumed if comparing our 100 or 1000 years closure depths to the engineering methods [*Stive et al.,* 1991]. This comparison emphasizes that closure predicted for short-term engineering projects should be shallower than those applicable for decadal to geologic coastal change.

4.3. Discussion of Application

Each site we analyzed had multiple profiles that, across tens of kilometers of coastline, share similar slopes, particularly over the first 20 m and often extending to 40 m or more (Figure 12). This local similarity of shoreface geometry, both in elevation and slope, suggests some form of active process control or underlying relict processes. At greater depths, transition to a flatter shelf slope is visually apparent at all of the passive coasts; the gross morphology at these depths is likely little affected by shoreline processes and is perhaps influenced by geologic constraints and sea level rise history. Most shelf features are below our calculated morphodynamic depth of closure, and morphologic evolution of the bed by processes included in our model would be geologically slow, even if wave-driven sediment transport occurs. Other processes, such as geostrophic flows [*Niedoroda and Swift*, 1991] or wave-supported gravity flows [*Friedrichs and Wright*, 2004] characteristic of active margins such as the Eel River, could control morphologic evolution.

Calculated values of representative wave heights range significantly across the different sites, and even sites with similar mean wave climates can have different effective wave heights depending on the influence of storm waves. In all cases, the calculated morphodynamic depths of closure are deeper than those computed using engineering formulae of *Hallermeier* [1981] (Figure 14). However, the visual coincidence of computed closure depth with the offshore break in slope suggests that the active shoreface is deeper than often considered by engineering practice.

We have chosen specific equations to describe wave asymmetry and mean drift as the primary drivers of sediment transport along with orbital velocity in the shoreface. There are several other equations and processes that could have been modeled instead that would change the magnitude and potentially the direction of u_1 and u_2. Our analysis may highlight that for passive coasts other processes are of greater importance in shoreface evolution than wave asymmetry or Stokes drift. Moreover, including waves that are not

shore normal in the analysis could temper and decrease the magnitude of the predicted characteristic morphodynamic wave conditions, thus decreasing the predicted MDOC. However, it is unlikely that the larger wave conditions are commonly more than 20° from shore normal.

5. Summary and Conclusions

We investigated an energetics-based formula for wave-driven cross-shore sediment flux and shoreface evolution using both shallow water wave assumptions (as has been done previously) and linear Airy wave theory (a new approach). Although similar equilibrium profiles are computed when using linear or shallow water wave assumptions, estimations of sediment flux with increasing depth diverge significantly. Both methods, using linear Airy wave theory or shallow water wave assumptions, predict diffusive profile evolution through morphodynamic Péclet number analysis, which we use to estimate a morphodynamic depth of closure, beyond which evolution of the shoreface is geologically slow. Although grain size affects the equilibrium slope, the computed morphodynamic depths of closure depend only on wave height and wave period; there is no dependence on grain size.

Our general approach is to understand the order of magnitude of wave-driven sediment transport processes to characterize the potential envelope of the time and depth dependence of shoreface evolution. Our method provides a novel means to estimate a depth of closure. In our definition, the depth of closure does not depend on cessation of sediment transport but rather attempts to quantify a depth beyond which the evolution of the shoreface in response to the shoreline becomes geologically slow.

The calculation of a characteristic morphodynamic wave value from a large data set of hindcasted wave heights (from WIS virtual buoys) also represents a useful tool for both regulators and scientists—it enables the parameterization of data for model inputs looking at the shoreface response to sea level rise. The magnitude-frequency analysis highlights the importance of large, infrequent wave conditions on shoreface profile evolution. The comparison of our formulation and approach to sites highlights that, overall, there is reasonable agreement between our calculations of equilibrium profiles, actual profiles, and our calculated morphodynamic depth of closure, with improved fits for active coasts, suggesting that inheritance may play a significant role in the shape of shorefaces on passive margin shelves.

Following previous examples, we used an energetics approach here, but there are many other approaches to compute sediment transport, for example, those based on bed shear stress [*Madsen*, 1991]. Although the energetics formulations for sediment transport do not encompass all processes occurring within the wave boundary layer, they are useful for our objective, which is to present gross quantification of the shoreface transition based upon the magnitude of wave-driven sediment transport by studying perturbations around a steady state. The main phenomena leading to our suggested morphologic depth of closure are the decay of wave influence with depth and a characteristic scale set by profile geometries. The robust nature of our general methodology suggests that different equations of sediment transport could be substituted in similar calculations, allowing for repeatability.

Notation List

β	slope, m/m
ρ	fluid density, g/cm^3
ρ_s	sediment density, g/cm^3
C_s	bed friction factor
D	diffusivity, m^2/s
D_c	diffusion coefficient, m^2/s^2
e_s	suspended sediment efficiency factor
g	acceleration of gravity, m/s^2
H	wave height, m
H_0	deep water wave height, m
K	sediment transport coefficient, s^2/m
k	wave number, m^{-1}
L	wavelength, m

l	characteristic length scale, m
L_0	deep water wavelength, m
q_s	cross-shore suspended sediment transport flux, m^2/s
u_i	wave velocity components, m/s
u_i'	derivative of wave velocity component
V	kinematic celerity, m/s
V_c	advection coefficient, m/s^2
w_s	sediment fall velocity, m/s
x_{eq}	steady state profile distance to shore, m
z	water depth, m

Acknowledgments

This manuscript has been greatly improved by detailed comments from three anonymous reviewers and Peter Ruggiero. Special thanks to Carl Friedrichs for providing the Eel River data used in Figure 11. We also thank Jorge Lorenzo-Trueba, Jeff Donnelly, and Rob Evans for fruitful discussions. Data supporting Figures 8–14 are available from the Wave Information Studies at http://wis.usace.army.mil/ and from the Marine Geoscience Data System within the GeoMapApp (http://www.geomapapp.org/). The MatLab code for the theoretical approach is available on Community Surface Dynamics Modeling System (CSDMS) as part of the coastal model repository (http://csdms.colorado.edu/wiki/Model:Cross_Shore_Sediment_Flux). This research has been supported by the National Science Foundation grant CNH-0815875, the Strategic Environment Research and Development Program, and the Coastal Ocean Institute of the Woods Hole Oceanographic Institution.

References

Aagaard, T. (2014), Sediment supply to beaches: Cross-shore sand transport on the lower shoreface, *J. Geophys. Res. Earth Surf.*, *119*, 913–926, doi:10.1002/2013JF003041.

Aagaard, T., and P. Sørensen (2012), Coastal profile response to sea level rise: A process-based approach, *Earth Surf. Processes Landforms*, *37*(3), 354–362, doi:10.1002/esp.2271.

Abreu, T., P. A. Silva, F. Sancho, and A. Temperville (2010), Analytical approximate wave form for asymmetric waves, *Coastal Eng.*, *57*(7), 656–667.

Ashton, A. D., and L. Giosan (2011), Wave-angle control of delta evolution, *Geophys. Res. Lett.*, *38*, L13405, doi:10.1029/2011GL047630.

Ashton, A. D., and A. B. Murray (2006), High-angle wave instability and emergent shoreline shapes: 1. Modeling of sand waves, flying spits, and capes, *J. Geophys. Res.*, *111*, F04011, doi:10.1029/2005JF000422.

Ashton, A. D., and A. C. Ortiz (2011), Overwash controls coastal barrier response to sea-level rise, in *Coastal Sediments*, vol. 13, pp. 230–243, ASCE, Miami, Fla.

Ashton, A. D., M. J. A. A. Walkden, and M. E. Dickson (2011), Equilibrium responses of cliffed coasts to changes in the rate of sea level rise, *Mar. Geol.*, *284*(1–4), 217–229, doi:10.1016/j.margeo.2011.01.007.

Bagnold, R. A. (1963), Mechanics of marine sedimentation, in *Physics of Sediment Transport by Wind and Water*, vol. 3, edited by M. N. Hill, pp. 188–230, John Wiley, New York.

Bailard, J. A. (1981), An energetics total load sediment transport model for a plane sloping beach, *J. Geophys. Res.*, *86*, 10,938–10,954, doi:10.1029/JC086iC11p10938.

Birkemeier, W. A. (1985), Field data on seaward limit of profile change, *J. Waterw. Port Coastal Ocean Eng.*, *111*(3), 598–602, doi:10.1061/(ASCE)0733-950X(1985)111:3(598).

Bowen, A. J. (1980), Simple models of nearshore sedimentation; beach profiles and longshore bars, edited by S. B. McCann, The Coastline of Canada, *Geol. Surv. Can. Pap., 80–10*, pp. 1–11.

Bray, M. J., and J. M. Hooke (1997), Prediction of soft-cliff retreat with accelerating sea-level rise, *J. Coastal Res.*, *13*(2), 453–467, doi:10.2307/4298640.

Brunsden, D., and J. B. Thornes (1979), Landscape sensitivity and change, *Trans. Inst. Br. Geogr.*, *4*(4), 463–484.

Bruun, P. (1962), Sea level rise as a cause of shore erosion, *J. Waterw. Harbors Div. Am. Soc. Civ. Eng.*, *88*(WW1), 13.

Bruun, P. (1983), Review of conditions for uses of the Bruun rule of erosion, *Coastal Eng.*, *7*(1), 77–89, doi:10.1016/0378-3839(83)90028-5.

Bruun, P. (1988), The Bruun rule of erosion by sea-level rise: A discussion on large-scale two- and three-dimensional usages, *J. Coastal Res.*, *4*(4), 627–648.

Cooper, J. A. G., and O. H. Pilkey (2004), Sea-level rise and shoreline retreat: Time to abandon the Bruun Rule, *Global Planet. Change*, *43*(3–4), 157–171, doi:10.1016/j.gloplacha.2004.07.001.

Cowell, P. J., P. S. Roy, and R. A. Jones (1995), Simulation of large-scale coastal change using a morphological behaviour model, *Mar. Geol.*, *126*(1–4), 45–61, doi:10.1016/0025-3227(95)00065-7.

Cowell, P. J., M. J. F. Stive, A. W. Niedoroda, H. J. De Vriend, D. J. P. Swift, G. M. Kaminsky, and M. Capobianco (2006a), The coastal-tract (part 1): A conceptual approach to aggregated modeling of low-order coastal change, *J. Coastal Res.*, *19*(4), 812–827, doi:10.2307/4299222.

Cowell, P. J., et al. (2006b), The coastal-tract (part 2): Applications of aggregated modeling of lower-order coastal change, *J. Coastal Res.*, *19*(4), 828–848.

Davidson-Arnott, R. G. D. (2005), Conceptual model of the effects of sea level rise on sandy coasts, *J. Coastal Res.*, *21*(6), 1166–1172, doi:10.2112/03-0051.1.

Dean, R. G. (1991), Equilibrium beach profiles: Characteristics and applications, *J. Coastal Res.*, *7*(1), 53–84.

Dean, R. G. (2002), *Beach Nourishment: Theory and Practice*, *Adv. Ser. on Ocean Eng.*, World Sci, Singapore.

Dean, R. G., and R. A. Dalrymple (1991), *Water Wave Mechanics for Engineers and Scientists*, *Adv. Ser. on Ocean Eng.*, vol. 2, World Sci., Singapore.

Dean, R. G., and E. M. Maurmeyer (1983), Models for beach profile response, in *CRC Handbook of Coastal Processes and Erosion*, edited by P. D. Komar, pp. 151–165, CRC Press, Boca Raton, Fla.

Dickson, M. E., C. S. Bristow, D. M. Hicks, H. Jol, J. Stapleton, and D. Todd (2009), Beach volume on an eroding sand-gravel coast determined using ground penetrating radar, *J. Coastal Res.*, *25*, 1149–1159, doi:10.2112/08-1137.1.

Donnelly, C., N. Kraus, and M. Larson (2006), State of knowledge on measurement and modeling of coastal overwash, *J. Coastal Res.*, *22*, 965–991, doi:10.2112/04-0431.1.

Dott, R. H., Jr., and J. Bourgeois (1982), Hummocky stratification: Significance of its variable bedding sequences, *Geol. Soc. Am. Bull.*, *93*(8), 663–680, doi:10.1130/0016-7606(1982)93<663:HSSOIV>2.0.CO;2.

Duke, W. L. (1985), Hummocky cross-stratification, tropical hurricanes, and intense winter storms, *Sedimentology*, *32*(2), 167–194, doi:10.1111/j.1365-3091.1985.tb00502.x.

Fenneman, N. M. (1902), Development of the profile of equilibrium of the subaqueous shore terrace, *J. Geol.*, *10*(1), 1–32.

Fredsoe, J., and R. Deigaard (1992), in *Mechanics of Coastal Sediment Transport*, edited by P. L.-F. Liu, World Sci, Singapore.

Friedrichs, C. T., and L. D. Wright (2004), Gravity-driven sediment transport on the continental shelf: Implications for equilibrium profiles near river mouths, *Coastal Eng.*, *51*(8–9), 795–811, doi:10.1016/j.coastaleng.2004.07.010.

Hallermeier, R. J. (1978), Uses for a calculated limit depth to beach erosion, in *Coastal Engineering Proceedings*, pp. 1493–1512, Am. Soc. of Civil Eng. (ASCE), New York.

Hallermeier, R. J. (1981), A profile zonation for seasonal sand beaches from wave climate, *Coastal Eng.*, *4*, 253–277.
Haxby, W. F. (2012), GeoMapApp. [Available from www.geomapapp.org.]
Holthuijsen, L. H. (2007), *Waves in Oceanic and Coastal Waters*, Cambridge Univ. Press, Cambridge, U. K.
Hutton, E. W. H., and J. P. M. Syvitski (2008), Sedflux 2.0: An advanced process-response model that generates three-dimensional stratigraphy, *Comput. Geosci.*, *34*(10), 1319–1337, doi:10.1016/j.cageo.2008.02.013.
Jenkins, S. A., and D. L. Inman (2006), Thermodynamic solutions for equilibrium beach profiles, *J. Geophys. Res.*, *111*, C02003, doi:10.1029/2005JC002899.
Jensen, R. E. (2010), *Wave Information Studies*, edited by U. S. A. C. of Engineers. [Available from http://wis.usace.army.mil/WIS_Documentation.shtml#ref.]
Jimenez, J., and A. Sanchez-Arcilla (2004), A long-term (decadal scale) evolution model for microtidal barrier systems, *Coastal Eng.*, *51*(8–9), 749–764, doi:10.1016/j.coastaleng.2004.07.007.
Jin, D., A. D. Ashton, and P. Hoagland (2013), Optimal responses to shoreline changes: An integrated economic and geologic model with applications to curved coasts, *Nat. Resour. Model.*, *26*(4), 572–604, doi:10.1111/nrm.12014.
Kemp, A. C., B. P. Horton, J. Donnelly, M. E. Mann, M. Vermeer, and S. Rahmstorf (2011), Climate related sea-level variations over the past two millennia, *Proc. Natl. Acad. Sci. U.S.A.*, *108*(27), 11,017–11,022, doi:10.1073/pnas.1015619108.
Kleinhans, M. G. (2002), *Sediment Dynamics on the Shoreface and Upper Continental Shelf: A Review*, Utrecht Univ, Utrecht, Netherlands.
Komar, P. D. (1991), The response of beaches to sea-level changes: A review of predictive models, *J. Coastal Res.*, *7*(3), 895–921.
Larson, M., N. C. Kraus, and N. C. Kraus (1995), Prediction of cross-shore sediment transport at different spatial and temporal scales, *Mar. Geol.*, *126*(1–4), 111–127, doi:10.1016/0025-3227(95)00068-A.
Lentz, S. J., M. Fewings, P. Howd, J. Fredericks, and K. Hathaway (2008), Observations and a model of undertow over the inner continental shelf, *J. Phys. Oceanogr.*, *38*(11), 2341–2357.
Leont'yev, I. O. (2012), Modeling beach profile evolution at centennial to millennial scales, *Mar. Geol.*, *52*(4), 550–560, doi:10.1134/S0001437012040054.
Limber, P. W., A. Brad Murray, P. N. Adams, and E. B. Goldstein (2014), Unraveling the dynamics that scale cross-shore headland relief on rocky coastlines: 1. Model development, *J. Geophys. Res. Earth Surf.*, *119*, 854–873, doi:10.1002/2013JF002950.
List, J. H., A. H. Sallenger, M. E. Hansen, and B. E. Jaffe (1997), Accelerated relative sea-level rise and rapid coastal erosion: Testing a causal relationship for the Louisiana barrier islands, *Mar. Geol.*, *140*(3–4), 347–365, doi:10.1016/S0025-3227(97)00035-2.
Longuet-Higgins, M. S. (1958), The mechanics of the boundary layer near the bottom in a progressive wave, in *Proceedings of the 6th International Conference on Coastal Engineering, ASCE*, pp. 184–193, The council on Wave Research, Richmond, Calif.
Lorenzo-Trueba, J., and A. D. Ashton (2014), Rollover, drowning, and discontinuous retreat: Distinct modes of barrier response to sea-level rise arising from a simple morphodynamic model, *J. Geophys. Res. Earth Surf.*, *119*, 779–801, doi:10.1002/2013JF002941.
Madsen, O. S. (1991), Mechanics of cohesionless sediment transport in coastal waters, in *Coastal Sediments*, pp. 15–27, ASCE, New York.
Malarkey, J., and A. G. Davies (2012), Free-stream velocity descriptions under waves with skewness and asymmetry, *Coastal Eng.*, *68*, 78–95.
McCave, I. N. (1985), Sedimentology: Hummocky sand deposits generated by storms at sea, *Nature*, *313*(6003), 533, doi:10.1038/313533b0.
Ministry of Economy, Trade, and Industry, and National Aeronautics and Space Administration (2011), ASTER Global Digital Elevation Map. [Available at: http://asterweb.jpl.nasa.gov/gdem.asp, Accessed 14 July 2014.]
Moore, L. J., J. H. List, S. J. Williams, and D. Stolper (2010), Complexities in barrier island response to sea level rise: Insights from numerical model experiments, North Carolina Outer Banks, *J. Geophys. Res.*, *115*, F03004, doi:10.1029/2009JF001299.
Nicholls, R. J., W. A. Birkemeier, and R. J. Hallermeier (1996), Application of the depth of closure concept, in *Coastal Engineering Proceedings*, pp. 3874–3887, New York.
Nicholls, R. J., W. A. Birkemeier, and G. Lee (1998), Evaluation of depth of closure using data from Duck, NC, USA, *Mar. Geol.*, *148*(3–4), 179–201, doi:10.1016/S0025-3227(98)00011-5.
Nichols, G. (1999), *Sedimentology and Stratigraphy*, Blackwell, Oxford, U. K.
Niedoroda, A. W., and D. J. P. Swift (1991), Shoreface processes, in *Handbook of Coastal and Ocean Engineering*, pp. 736–769, Gulf Company, Houston, Tex.
Patterson, D. (2012), Shoreward sand transport outside the surfzone, northern Gold Coast, Australia, *Coastal Eng. Proc.*, *1*(33), 1–15, doi:10.9753/icce.v33.sediment.26.
Pelletier, J. D., and T. Perron (2012), Analytic solution for the morphology of a soil-mantled valley undergoing steady headward growth: Validation using case studies in southeastern Arizona, *J. Geophys. Res.*, *117*, F02018, doi:10.1029/2011JF002281.
Perron, J. T., W. E. Dietrich, and J. W. Kirchner (2008), Controls on the spacing of first-order valleys, *J. Geophys. Res.*, *113*, F04016, doi:10.1029/2007JF000977.
Peters, S. E., and D. P. Loss (2012), Storm and fair-weather wave base: A relevant distinction?, *Geology*, *40*(6), 511–514, doi:10.1130/G32791.1.
Pilkey, O. H., J. A. G. Cooper, and D. A. Lewis (2009), Global distribution and geomorphology of fetch-limited barrier islands, *J. Coastal Res.*, *25*, 819–837, doi:10.2112/08-1023.1.
Pritchard, D., G. G. Roberts, N. J. White, and C. N. Richardson (2009), Uplift histories from river profiles, *Geophys. Res. Lett.*, *36*, L24301, doi:10.1029/2009GL040928.
Ranasinghe, R., T. M. Duong, S. Uhlenbrook, D. Roelvink, and M. J. F. Stive (2012), Climate-change impact assessment for inlet-interrupted coastlines, *Nat. Clim. Change*, *3*(1), 83–87, doi:10.1038/nclimate1664.
Rienecker, M. M., and J. D. Fenton (1981), A Fourier approximation method for steady water waves, *J. Fluid Mech.*, *104*, 119–137.
Ruessink, B. G., G. Ramaekers, and L. C. Van Rijn (2012), On the parameterization of the free-stream non-linear wave orbital motion in nearshore morphodynamic models, *Coastal Eng.*, *65*, 56–63.
Sageman, B. B. (1996), Lowstand tempestites: Depositional model for Cretaceous skeletal limestones, Western Interior basin, *Geology*, *24*(10), 888–892, doi:10.1130/0091-7613(1996)024<0888:LTDMFC>2.3.CO;2.
Sherwood, C. R., J. W. Long, P. J. Dickhudt, P. S. Dalyander, D. M. Thompson, and N. G. Plant (2014), Inundation of a barrier island (Chandeleur Islands, Louisiana, U.S.A.) during a hurricane: Observed water-level gradients and modeled seaward sand transport, *J. Geophys. Res. Earth Surf.*, *119*, 1498–1515, doi:10.1002/2013JF003069.
Soulsby, R. L. (2006), *Simplified Calculation of Wave Orbital Velocities*, HR Wallingford Ltd., Wallingford, U. K.
Stive, M. J. F., and H. J. de Vriend (1995), Modelling shoreface profile evolution, *Mar. Geol.*, *126*(1–4), 235–248, doi:10.1016/0025-3227(95)00080-I.
Stive, M. J. F., R. J. Nicholls, and H. J. De Vriend (1991), Sea-level rise and shore nourishment: A discussion, *Coastal Eng.*, *16*(1), 147–163, doi:10.1016/0378-3839(91)90057-N.
Stolper, D., J. H. List, and E. R. Thieler (2005), Simulating the evolution of coastal morphology and stratigraphy with a new morphological-behaviour model (GEOMBEST), *Mar. Geol.*, *218*, 17–36, doi:10.1016/j.margeo.2005.02.019.

Sullivan, T., and W. Lucas (2007), Chronic misapplication of the relationship between magnitude and frequency in geomorphic processes, as illustrated in Fluvial Processes in Geomorphology by Leopold, Wolman and Miller (1964), in *Advancing the Fundamental Sciences: Proceedings of the Forest Service National Earth Sciences Conference*, pp. 133–135, U.S. Dep. of Agric., For. Serv., Pac. Northwest Res. Stn., Portland, Oreg.

Swenson, J. B., C. Paola, L. Pratson, V. R. Voller, and A. B. Murray (2005), Fluvial and marine controls on combined subaerial and subaqueous delta progradation: Morphodynamic modeling of compound-clinoform development, *J. Geophys. Res.*, *110*, F02013, doi:10.1029/2004JF000265.

Swift, D. J. P., A. W. Niedoroda, C. E. Vincent, and T. S. Hopkins (1985), Barrier island evolution, middle Atlantic shelf, U.S.A. Part I: Shoreface dynamics, *Mar. Geol.*, *63*(1–4), 331–361, doi:10.1016/0025-3227(85)90089-1.

Thieler, E. R., A. L. Brill, W. J. Clearly, C. H. Hobbs III, and R. A. Gammisch (1995), Geology of the Wrightsville Beach, North Carolina shoreface: Implications for the concept of shoreface profile of equilibrium, *Mar. Geol.*, *126*(1–4), 271–287, doi:10.1016/0025-3227(95)00082-A.

Thieler, E. R., O. H. Pilkey, W. J. Clearly, and W. C. Schwab (2001), Modern sedimentation on the shoreface and inner continental shelf at Wrightsville Beach, North Carolina, USA, *J. Sediment. Res.*, *71*(6), 958–970, doi:10.1306/032101710958.

Vermeer, M., and S. Rahmstorf (2009), Global sea level linked to global temperature, *Proc. Natl. Acad. Sci. U.S.A.*, *106*(51), 21,527–21,532, doi:10.1073/pnas.0907765106.

Wallace, D. J., J. B. Anderson, and R. A. Fernández (2010), Transgressive ravinement versus depth of closure: A geological perspective from the upper Texas coast, *J. Coastal Res.*, *26*, 1057–1067, doi:10.2112/JCOASTRES-D-10-00034.1.

Wolinsky, M. A. (2009), A unifying framework for shoreline migration: 1. Multiscale shoreline evolution on sedimentary coasts, *J. Geophys. Res.*, *114*, F01008, doi:10.1029/2007JF000855.

Wolman, M. G., and R. Gerson (1978), Relative scales of time and effectiveness of climate in watershed geomorphology, *Earth Surf. Processes*, *3*, 189–208, doi:10.1002/esp.3290030207.

Wolman, M. G., and J. P. Miller (1960), Magnitude and frequency of forces in geomorphic processes, *J. Geol.*, *68*(1), 54–74.

Wright, L. D., J. D. Boon, S. C. Kim, and J. H. List (1991), Modes of cross-shore sediment transport on the shoreface of the Middle Atlantic Bight, *Mar. Geol.*, *96*, 19–51, doi:10.1016/0025-3227(91)90200-N.

Zenkovitch, V. P. (1946), On the study of shore dynamics, *Trans. Inst. Okeanol., Akad. Nauk SSSR*, *1*, 99–112.

Zhang, K., B. C. Douglas, and S. P. Leatherman (2004), Global warming and coastal erosion, *Clim. Change*, *64*(1–2), 41–58, doi:10.1023/B:CLIM.0000024690.32682.48.